Received: 9 October 2023 | Revised: 12 March 2024 | Accepted: 2 April 2024

DOI: 10.1002/alz.13857

Alzheimer's & Dementia®
THE JOURNAL OF THE ALZHEIMER'S ASSOCIATION

RESEARCH ARTICLE

A TrkB and TrkC partial agonist restores deficits in synaptic function and promotes activity-dependent synaptic and microglial transcriptomic changes in a late-stage Alzheimer's mouse model

Amira Latif-Hernandez[1] | **Tao Yang**[1] | **Robert R. Butler III**[1] | **Patricia Moran Losada**[1,2] | **Paras S. Minhas**[1] | **Halle White**[1] | **Kevin C. Tran**[1] | **Harry Liu**[1] | **Danielle A. Simmons**[1] | **Vanessa Langness**[1] | **Katrin I. Andreasson**[1,2,3] | **Tony Wyss-Coray**[1,2,4] | **Frank M. Longo**[1,2]

[1]Department of Neurology & Neurological Sciences, Stanford University School of Medicine, Palo Alto, California, USA

[2]Wu Tsai Neurosciences Institute, Stanford University, Stanford, California, USA

[3]Chan Zuckerberg Biohub, San Francisco, California, USA

[4]The Phil and Penny Knight Initiative for Brain Resilience, Stanford University, Stanford, California, USA

Correspondence
Amira Latif-Hernandez, Department of Neurology and Neurological Sciences, Stanford University School of Medicine, 300 Pasteur Drive, Palo Alto, CA 94304, USA.
Email: amiralh@stanford.edu

Funding information
NIH, Grant/Award Numbers: P30AG10161, P30AG72975, R01AG15819, R01AG17917, R01AG036836, U01AG46152, U01AG61356, U01AG046139, P50 AG016574, R01 AG032990, U01AG046139, R01AG018023, U01AG006576, U01AG006786, R01AG025711, R01AG017216, R01AG003949, R01NS080820, U24NS072026, P30AG19610, U01AG046170, RF1AG057440, U24AG061340; Cure PSP; Mayo; Michael J Fox foundations; Arizona Department of Health Services; Arizona Biomedical Research Commission; Scully Family Initiative; Taube Family Foundation; Jean Perkins Foundation; Applebaum Foundation; Horngren Family; 5T32GM007365-45; Stanford Alzheimer's Disease Research Center, Grant/Award Numbers: P30 AG066515, SPO 147289

Abstract

INTRODUCTION: Tropomyosin related kinase B (TrkB) and C (TrkC) receptor signaling promotes synaptic plasticity and interacts with pathways affected by amyloid beta (Aβ) toxicity. Upregulating TrkB/C signaling could reduce Alzheimer's disease (AD)-related degenerative signaling, memory loss, and synaptic dysfunction.

METHODS: PTX-BD10-2 (BD10-2), a small molecule TrkB/C receptor partial agonist, was orally administered to aged London/Swedish-APP mutant mice ($APP^{L/S}$) and wild-type controls. Effects on memory and hippocampal long-term potentiation (LTP) were assessed using electrophysiology, behavioral studies, immunoblotting, immunofluorescence staining, and RNA sequencing.

RESULTS: In $APP^{L/S}$ mice, BD10-2 treatment improved memory and LTP deficits. This was accompanied by normalized phosphorylation of protein kinase B (Akt), calcium-calmodulin–dependent kinase II (CaMKII), and AMPA-type glutamate receptors containing the subunit GluA1; enhanced activity-dependent recruitment of synaptic proteins; and increased excitatory synapse number. BD10-2 also had potentially favorable effects on LTP-dependent complement pathway and synaptic gene transcription.

DISCUSSION: BD10-2 prevented $APP^{L/S}$/Aβ-associated memory and LTP deficits, reduced abnormalities in synapse-related signaling and activity-dependent

Tao Yang, Robert R. Butler III, and Patricia Moran Losada contributed equally to this study.

[Correction added on June 9, 2024, after first online publication: The middle initial and last name for the author has been corrected from Robert Raymond-Butler III to Robert R Butler III.]

transcription of synaptic genes, and bolstered transcriptional changes associated with microglial immune response.

KEYWORDS
activity-dependent gene expression, amyloid beta-induced synaptic dysfunction, tropomyosin related kinase B and C receptor signaling

Highlights

- Small molecule modulation of tropomyosin related kinase B (TrkB) and C (TrkC) restores long-term potentiation (LTP) and behavior in an Alzheimer's disease (AD) model.
- Modulation of TrkB and TrkC regulates synaptic activity-dependent transcription.
- TrkB and TrkC receptors are candidate targets for translational therapeutics.
- Electrophysiology combined with transcriptomics elucidates synaptic restoration.
- LTP identifies neuron and microglia AD-relevant human-mouse co-expression modules.

1 | BACKGROUND

Synaptic dysfunction and eventual loss of synapses are fundamental contributors to cognitive deficits in Alzheimer's disease (AD).[1,2] Other key neuropathological features of AD include accumulation of toxic species of amyloid beta (Aβ) and tau proteins. Pathological Aβ and tau attenuate hippocampal long-term potentiation (LTP) in AD mouse models.[3–5] LTP is a form of synaptic plasticity involved in memory and learning. LTP impairments induced by Aβ and tau can be explained, in part, by disrupted neurotrophin signaling.[6–11] The neurotrophin brain-derived neurotrophic factor (BDNF) is released in an activity-dependent manner in the hippocampus. BDNF binds to and activates tropomyosin related kinase B (TrkB) receptors. Upon activation, TrkB translocates to the post-synaptic terminal[12] and initiates signaling cascades including the phosphatidylinositol-3 kinase (PI3K)/protein kinase B (Akt) and phospholipase Cy-1 (PLCγ)/protein kinase C (PKC) pathways, which mediate LTP maintenance and support synaptic transmission and membrane excitability.[13] Synaptic plasticity is also facilitated by the neurotrophin NT-3, and signaling via its receptor, TrkC.[14,15] Deficiencies in BDNF/TrkB and NT-3/TrkC signaling have been observed in the brains of AD patients and mouse models, and have been associated with Aβ and tau accumulation, synapse loss, and cognitive decline.[16–18] TrkB/TrkC signaling pathways largely intersect molecular pathways essential to Aβ and tau pathology and contribute to synaptic plasticity.[19] Thus, activating TrkB/TrkC signaling may counteract AD-related degenerative signaling and restore LTP. The development of small-molecule TrkB agonists and modulators has emerged as a key therapeutic strategy[20–22] as the use of BDNF itself as a therapeutic is hampered by its unfavorable pharmacokinetic properties.[23] While limited research exists on the concomitant activation of TrkB and TrkC receptors using small molecule compounds,[24,25] the present study addresses this gap.

Previously, we identified a small molecule parent compound, LM22B-10, that activates TrkB and TrkC in vitro[24] and in vivo (unpublished and in Simmons et al.[26]). Activated downstream signaling pathways include PI3K/Akt, mitogen-activated protein kinase/extracellular signal-regulated kinase (MAPK/ERK), and PLCγ/PKC and this signaling is associated with the prevention of dendritic spine loss in aged mice.[24] A derivative of LM22B-10, designated as PTX-BD10-2 (BD10-2), was developed which has improved blood–brain barrier penetration after oral administration and reverses cholinergic neuron atrophy associated with pathological tau, identified by AT8 antibody, in late-stage $APP^{L/S}$ mice.[25]

In the present investigation, we examined whether promoting TrkB and TrkC signaling with the small molecule ligand BD10-2 can reduce measures of synaptic integrity decline observed in the $hAPP^{Lond/Swe}$ ($APP^{L/S}$) mouse model of AD. Upregulation of TrkB and C signaling might preserve synaptic integrity regardless of whether deficiencies in levels of BDNF/NT-3 and/or TrkB/C signaling are present prior to the initiation of treatment. BD10-2 was orally administered to $APP^{L/S}$ mice with memory deficits and late-stage amyloid pathology.[27,28] This therapeutic strategy was adopted to increase clinical relevance as therapeutic trials are generally initiated when key elements of pathology are already established. We found that BD10-2 significantly reduced memory and LTP impairments, as well as synaptic- and neurotrophin-related signaling deficits in $APP^{L/S}$ mice. These beneficial effects may be explained in part by BD10-2's ability to normalize alterations in activity-dependent transcription of synaptic genes that were observed in vehicle (Veh)-treated $APP^{L/S}$ mice. Additionally, we identified upregulation of genes in pathways associated with microglia and immune responses in $APP^{L/S}$ mice that were further upregulated in $APP^{L/S}$ mice treated with BD10-2 suggesting that BD10-2 may enhance one or more elements of the existing immune response to AD-related pathology.

2 | METHODS

2.1 | Reagents

LM22B-10 (2-[[4-[[4-[Bis-(2-hydroxy-ethyl)-amino]-phenyl]-(4-chloro-phenyl)-methyl]-phenyl]-(2-hydroxy-ethyl)-amino]-ethanol) and PTX-BD10-2 (BD10-2) (Bis-{4-[bis-(2-methoxy-ethyl)-amino]-phenyl}-ethane) were custom manufactured for our laboratory by Ricerca Biosciences LLC. The compounds were characterized by high-performance liquid chromatography, and liquid chromatography/mass spectrometry and had a purity of ≥ 97%. Recombinant BDNF was purchased from PeproTech. Other reagents were purchased from Sigma-Aldrich, unless otherwise stated.

2.2 | NIH-3T3 cell cultures and cell survival assays

Mouse NIH-3T3 cells expressing TrkA (NIH-3T3-TrkA) and p75 (NIH-3T3-p75) were provided by Dr. William Mobley (University of California San Diego), and NIH-3T3 cells expressing TrkB (NIH-3T3-TrkB) or TrkC (NIH-3T3-TrkC) were provided by Dr. David Kaplan (University of Toronto). Cells were propagated in Dulbecco's Modified Eagle Medium (DMEM) supplemented with 10% fetal bovine serum (Invitrogen) and 200–400 µg/mL Geneticin. Cells were seeded onto 24-well plates (30,000 cells/well) and cultured in medium consisting of 50% phosphate-buffered saline (PBS) and 50% DMEM without supplements. After exposure to BDNF (20 ng/mL, 0.7 nM) or 10 to 1000 nM LM22B-10 or BD10-2 for 72 to 96 hours, cells were suspended in 50 µL lysis buffer, transferred to white, opaque 96-well culture plates and survival was measured using the ViaLight Assay (Lonza Group).

2.3 | Primary neuronal cultures and cell survival assays

Hippocampal neuron cultures were prepared from embryonic day 16 (E16) CF1 mouse fetuses, as described previously.[29] Under the low-density conditions used in the present studies, neuronal survival is dependent, in part, on addition of exogenous neurotrophins.[30,31] LM22B-10 and BD10-2 were dissolved in water with 2% to 3% of 1N HCl at a stock concentration of 10 mM prior to dilution (1:10,000) in culture medium. After 48 hours of exposure to BDNF, LM22B-10, or BD10-2, cells were immunostained for the neuron-specific marker, β-tubulin III (Tuj1), and cell survival was quantified by counting immunopositive, morphologically intact cell bodies.[31,32]

2.4 | Animals

All animal use procedures complied with the National Institutes of Health Guide for the Care and Use of Laboratory Animals and all protocols were approved by the Institutional Animal Care and Use Committee at Stanford University. These experiments used Thy1-hAPP$^{Lond/Swe}$ [Line 41] mice (APP$^{L/S}$), which express human APP751 containing the London (V7171) and Swedish (K670M/N671L) mutations under the control of the Thy-1 promoter.[27] Mice were bred in our laboratory and maintained on a C57BL/6 background. Mice were group housed in mixed genotypes. All mice received cotton nestlets and paper tubes. Water and food were freely available. Genotyping using tail DNA was performed by TransnetYX Inc. We chose male mice to minimize variability and simplify the experimental design, given the complexity of combining electrophysiological techniques, protein signaling analyses, and RNA-seq studies. We focus on genotype, drug, and stimulation effects, but we acknowledge the limitation and plan to explore sex as a factor in future studies.

RESEARCH IN CONTEXT

1. **Systematic review**: The authors extensively examined both conventional sources (e.g., PubMed) and meeting abstracts/presentations, referencing evidence regarding the role of tropomyosin related kinase B (TrkB) and C (TrkC) receptors in synaptic plasticity and potential involvement in synaptic dysfunction in Alzheimer's disease (AD) and AD models, all appropriately cited in the article.
2. **Interpretation**: We provide robust evidence that targeting TrkB and TrkC receptor activation in an AD mouse model ameliorates synaptic loss of function and degeneration with mechanisms that align with existing preclinical and clinical research.
3. **Future directions**: Further studies are needed to: (a) gain a deeper understanding of AD pathophysiology associated changes in activity-dependent transcription of synaptic and immune programs during long-term potentiation (LTP); (b) use these insights to identify novel therapeutic targets for AD and other neurodegenerative disorders; (c) evaluate the possibility of preventing, decreasing, or reversing LTP and cognition deficits through TrkB and TrkC modulation in early-stage AD.

2.5 | Study design for BD10-2 treatment of APP$^{L/S}$ mice

To examine the acute effects of BD10-2 on LTP, hippocampal slices were prepared from a group of male 16-month-old wild-type (WT; $n = 6$ mice) and APP$^{L/S}$ mice ($n = 6$ mice). BD10-2 was dissolved by agitation and sonication at 37°C in 25% hydroxypropyl-β-cyclodextrin (HPCD; Aldrich) in de-ionized water as the Veh. Hippocampal slices were exposed to 1000 nM BD10-2 or Veh via bath application. A separate group of male WT ($n = 34$) and APP$^{L/S}$ ($n = 44$) mice were administered Veh or BD10-2 (50 mg/kg, 10 mL/kg) once daily by oral gavage

(OG) 5 days/week as previously described[25] for 3 months starting at 13 months of age. A 2 × 2 study design was used with the following groups: WT-Veh (n = 17 mice), WT-BD10-2 (n = 17 mice), APP-Veh (n = 22 mice), and APP-BD10-2 (n = 22 mice). BD10-2 was administered to late-symptomatic $APP^{L/S}$ mice when extracellular Aβ deposits (present at age 3–5 months), tau pathology (present at age 6–8 months), and memory deficits (present at age 6–9 months) are well established.[25,27,28,33–35] After ≈ 2 months of treatment, memory-related performance in WT-Veh (n = 10 mice), WT-BD10-2 (n = 10 mice), APP-Veh (n = 9 mice), and APP-BD10-2 (n = 12 mice) mice was assessed using the novel object recognition (NOR), novel object displacement (NOD), and Barnes maze tests. Behavioral testing was performed daily, 24 hours after the last BD10-2 or Veh dose for ≈ 1.5 months. In a separate cohort dedicated to LTP measurements, mice were treated with BD10-2 or Veh (WT-Veh [n = 7 mice], WT-BD10-2 [n = 7 mice], APP-Veh [n = 13 mice], and APP-BD10-2 [n = 10 mice]) and hippocampal slices were harvested and prepared for electrophysiology recordings performed daily from two mice per day over a period of approximately 1 month at 16 months of age (+/− 2 weeks). Electrophysiology measures were conducted 24 hours after the last BD10-2 or Veh administration.

2.6 | NOR and displacement

The NOR and NOD tasks are based on the ability of mice to show preference for novel objects versus familiar objects when allowed to explore freely.[36] Mice were individually habituated to an open arena (50 cm × 50 cm, dim light, 24°C) 5 minutes prior to the training session with an inter-training interval of 3 minutes. During the training session, two identical objects were placed in the arena and the animals were allowed to explore for 10 minutes. During the testing session for NOD, after a delay of 24 hours, the animals were placed back into the same arena in which one of the objects used during training was moved to a new location in the arena. The mice were allowed to explore freely for 10 minutes. During the testing for NOR, the familiar object that remained in the same location on testing day 1 was replaced by a novel object of similar dimensions but with a different shape/color. The mice were allowed to explore freely for 10 minutes. Digital video tracking (using Kinovea software) of body movements and nose position was used to quantify the exploratory activity around the objects (2 cm zone around the objects). Exploration behavior was assessed by establishing the discrimination index (DI, as a percentage), that is, the ratio of the time spent exploring the novel object over the time spent exploring the two objects. A DI of ≥ 50% is therefore characteristic of training; significantly increased DI is characteristic of recognition. To evaluate memory, comparisons were made for each genotype/treatment group between the testing sessions (24 hours) and the training sessions (0 hours). Behavioral experiments were performed by experimenters blinded to genotype and treatment.

2.7 | Barnes maze

The Barnes maze is a spatial memory task in which a mouse must learn a target location (hole) to escape a brightly lit platform using distal cues. The experimental protocol was adopted from Attar et al.[37] with minor modifications. The maze consisted of a circular, white PVC slab (8 mm thick, 91.4 cm diameter) with 20 holes (7.62 cm diameter) along the perimeter 2.54 cm from the edge and mounted on a rotating stool 76.2 cm above the ground. Beneath the escape hole, a platform and ramp were located 5.08 cm below the surface of the maze leading to a mouse cage with darkened walls to reduce light. The maze was situated in the center of a room with two 120 W lights facing toward it to provide an aversive stimulus. Eight simple colored-paper shapes (squares, rectangles, and circles) were mounted on the walls of the room as visual cues. After testing each mouse, the maze was cleaned with 70% ethanol and rotated clockwise to avoid intra-maze odor or visual cues. All sessions were recorded using a JVC Everio HD camcorder GZ-E200 and analyzed with Kinovea video tracking software. The animals interacted with the Barnes maze in three phases: habituation (day 1), training (days 2–3), and probe (day 4). Before starting each session, mice were acclimated to the testing room for 1 hour. Then all mice from one cage (n = 4–5) were placed in individual holding cages where they remained until the end of their testing sessions each day. On habituation day, the mice were placed in the center of the maze within a vertically oriented black PVC pipe (10.2 cm diameter, 17.8 cm height) for 15 seconds and guided slowly to the hole that led to the escape cage over the course of 10 to 15 seconds. The mice were given 3 minutes to independently enter the target hole, and if they did not, they were nudged with the PVC pipe to enter. The 120 W lights were then shut off and mice were allowed to rest in the escape cage for 2 minutes. The training phase occurred 24 hours after the habituation phase and was split across two days (days 2 and 3), with three trials on the first day and two trials on the second day. During each trial, the mice were placed in the center of the maze within the PVC pipe for 15 seconds and after being allowed 3 minutes to explore the maze. If mice found and entered the target hole before 3 minutes passed, the lights were shut off and the training trial ended. Mice were allowed to rest in the escape cage for 2 minutes. If at the end of the 3 minutes the mice had not entered the target hole, they were nudged with the PVC pipe. A total of five trials were conducted. During each trial, latency (time) to enter the target hole as well as distance traveled were recorded. The probe phase occurred 24 hours after the training phase and was conducted on the last day (day 4). Mice were placed in the center of the maze within the PVC pipe for 15 seconds and after allowed 3 minutes to explore the maze. The probe session ended whenever the mouse entered the target hole or if 3 minutes had passed. During the probe phase, measures of time spent per quadrant, latency to enter the target hole, and distance traveled were recorded. Behavioral experiments were performed by experimenters blinded to genotype and treatment.

2.8 | Electrophysiology recordings

Electrophysiological recordings were performed in hippocampal slices as previously described.[38] WT-Veh, WT-BD10-2, APP-Veh, and APP-BD10-2 slices were randomized during the experiment. For experiments using chronically treated mice, brains were harvested, and hippocampal slices were prepared 24 hours after the final dose of BD10-2 or Veh. Animals were euthanized by cervical dislocation, the brain was removed, and the right hippocampus was rapidly dissected and placed into ice-cold (4°C) artificial cerebrospinal fluid (ACSF) and saturated with carbogen (95% O_2/5% CO_2). The composition of the ACSF was as follows (in mM): 124 NaCl, 4.9 KCl, 24.6 $NaHCO_3$, 1.20 KH_2PO_4, 2.0 $CaCl_2$, 2.0 $MgSO_4$, and 10.0 glucose, adjusted to a pH of 7.4. Transverse hippocampal slices were then prepared at a 350 µm thickness, from the dorsal region of the hippocampus using the McIlwain tissue chopper (Stoelting). These slices were transferred to a recovery chamber and maintained in oxygenated ACSF at room temperature for a minimum of 1.5 hours. Slices were then placed into a submerged-type chamber at 32°C where they were continuously perfused with ACSF at a flow rate of 1.5 mL/minute. Slices were delicately positioned onto an R6501A multi-electrode array (Alpha MED Scientific Inc.) arrayed in an 8 × 2 matrix with electrodes spaced an interpolar distance of 150 µm and each matrix measured at 50 µm × 50 µm. After a 30-minute incubation period, field excitatory postsynaptic potentials (fEPSPs) were recorded by stimulating downstream electrodes in the CA1 and CA3 regions along the Schaffer collateral pathway. The MED64 System (Alpha MED Scientific Inc.) was used to acquire signals. The time course of the fEPSP was determined using the descending slope function for all the experiments. Input/output curves were generated by gradually increasing stimulus currents in the pathway, ranging from 10 to 90 µA (in 5-µA increments), while monitoring evoked responses. Once the input/output curves were established, the stimulation strength was adjusted to maintain the fEPSP slope at 35% of its maximal value throughout the experiment. During the baseline recording, a single response was evoked at a 30 second interval for at least 20 minutes. To induce a strong form of LTP, three episodes of theta-burst stimulation (TBS) were used, with each TBS consisting of 10 bursts of four stimuli at 100 Hz separated by 200 ms (double pulse width). This was followed by a recording of evoked responses beginning 1 minute after LTP induction and continuing every 30 seconds for 120 minutes after TBS application, which marked the end of the experiment. The mean baseline fEPSP value was calculated and LTP was measured as the percentage change from baseline after TBS. Paired-pulse ratio (PPR) experiments were conducted, as previously described.[7,39] PPR responses to two impulses given at an interval of 10, 20, 50, 100, 200, or 500 ms were recorded. During baseline recording, three single stimuli (0.1 ms pulse width; 10 second intervals) were measured every 5 minutes and averaged for the 60 minute fEPSP values. For experiments examining acute effects of BD10-2, the TrkB/C ligand was dissolved in water with 2% to 3% of 1N HCl at a stock concentration of 10 mM prior to dilution to a final concentration of 100 nM in the ACSF bath. Compound and Veh solutions were added to oxygenated ACSF from 20 minutes before and until 130 minutes after TBS (see figures for details).

2.9 | Protein extraction and western blot analysis

Hippocampal slices with (120 minutes post-TBS) or without stimulation were lysed in RIPA lysis buffer (150 mM NaCl, 50 mM Tris, pH 7.4, 1 mM EDTA, 1% Triton X-100 or 1% NP40, 10% glycerol, 1 mM PMSF, Na3VO4 and protease inhibitor cocktail). Lysates were mixed with 4× NuPAGE lithium dodecyl sulfate loading buffer containing dithiothreitol. They were loaded (20–40 µg protein / lane) onto a NuPAGE 4% to 12% Bis-Tris gradient gel then transferred to PVDF membranes using 100 V for 1.5 hours. Membranes were incubated in blocking buffer for 1 hour at room temperature and then probed with primary antibodies. Antibodies consisted of: mouse monoclonal anti-phospho-ERK$^{T202/Y204}$ (1:2000, 9106), rabbit polyclonal anti-ERK (1:2000, 9101), mouse monoclonal anti-phospho-Akt^{S473} (1:2000, 4051), rabbit polyclonal anti-Akt (1:2000, 9272), rabbit polyclonal anti-phospho-calcium-calmodulin–dependent kinase II (CaMKII)^{Thr286} (1:2000, 12,716), rabbit polyclonal CaMKII (1:2000, 3362), rabbit monoclonal anti-phopho-GluA1^{Ser831} (1:2000, 75,574), and rabbit monoclonal GluA1 (1:2000, 13,185) purchased from Cell Signaling Technology, Inc.; mouse anti-monoclonal PSD-95 (1:3000, MAB1598) and synaptophysin (1:10,000, MAB329-C) and mouse monoclonal anti-actin (1:10,000, A5441) from Millipore Sigma. Primary antibody incubations were conducted overnight at 4°C followed by incubation with the appropriate horseradish peroxidase conjugated secondary antibody for 1 hour at room temperature. The immunobands were developed by incubating membranes in enhanced chemiluminescence developing solutions mixed in equal volumes for 1 minutes followed by imaging with Kodak film.

2.10 | Double immunofluorescence staining of hippocampal slices

After electrophysiology experiments, TBS (+) and TBS (–) hippocampal slices were post-fixed in 4% paraformaldehyde in PBS for 24 hours and transferred to 30% sucrose (Sigma-Aldrich). Using a freezing microtome, coronal slices were sectioned at 30 from 350 µm TBS (+) and TBS (–) hippocampal slices and stored at –20°C in cryoprotectant (20% glycerol, 30% ethylene glycol in phosphate buffer) until immunostaining. Slices were washed twice for 5 minutes in tris-buffered saline (Tris-BS; pH 7.6), pretreated with 0.4% TritonX-100 in Tris-BS, followed by a 1 hour incubation at room temperature in blocking solution (3% normal donkey serum, 0.4% TritonX-100, and 3% bovine serum in Tris-BS). Next, slices were incubated with primary antibodies for drebrin (1:1000, Enzo, Cat#ADI-NBA-110) and GLuA1 (AMPA receptor [AMPAR] 1, GLuA1, 1:400, Cell Signaling 13185), or antibodies for PSD-95 (1:500, MAB1598) and VGLUT1 (1:1000, 48-2400) in blocking buffer overnight at 4°C. They were then washed three times for 5 minutes and then incubated with secondary antibody Cy3-Donkey anti-rabbit (1:400) and FITC-Donkey anti-mouse (1:400) in Tris-BS for 4 hours. Hippocampal sections were mounted onto slides, coverslipped with Prolog Anti-Fade solution with DAPI, and imaged at least 48 hours later.

2.11 | Thioflavine S staining

For visualizing Aβ protein aggregates with Thioflavin S, free-floating 30 µm hippocampal slices, prepared as described above, were rinsed in PBS for 8 to 10 minutes followed by distilled water for 8 to 10 minutes. Subsequently, the sections were incubated for 8 minutes in Thioflavin S solution (1% Thioflavin S in 50% ethanol, filtered through 3 mm filter paper). Brain slices were sequentially washed in 80% and 95% ethanol for 1 minute. Finally, the sections were rinsed in distilled water for 15 minutes, then three washes in double-distilled water for 5 minutes each. Last, the slices were cover-slipped with Prolong mounting medium containing DAPI (Invitrogen).

2.12 | Fluorescence microscopy and quantitative image analysis

Fluorescent images of mouse hippocampal slices double-immunostained for GluA1 and drebrin, or VGlut1 and PSD-95 were obtained using a Leica DM550 or a Stellaris 5 confocal microscope (both Leica Microsystems). A 63× objective was used to obtain z-stack images (0.7 µm step size; 40 steps) of the CA1 region of the hippocampus containing the most synapses near the pyramidal cells; three images were taken per slice. The laser power, gain, and offset settings were adjusted using LAS-X viewer software (Leica) to optimize signal capture; identical settings were then applied to all subsequent images for a given staining set, each including all four genotype/treatment conditions. Images were deconvolved (50 iterations) using the batch processing function in Huygens Essential software so that the same parameter settings were used for each immunostaining analyzed. Colocalization of GluA1/drebrin, and VGlut1/PSD-95 was quantified using Huygens Essential software which calculated Manders coefficients (M1) and Spearman correlation, respectively.

To capture fibrillary Aβ staining in the entire hippocampal region, stitched 2D planar images were acquired using a 20× objective on a Stellaris 5 confocal microscope platform from Leica Microsystems. The hippocampus was covered in 20 tiles across the same z-plane, ensuring optimal signal intensity. Thioflavin S-positive area was quantified using ImageJ software. Briefly, images were converted to 8-bit grayscale. Within the Region of Interest (ROI) Manager, a ROI was manually drawn around the hippocampal slice, followed by background subtraction (50 pixels). Finally, the images were thresholded and percentage of area measured.

2.13 | Tissue processing for RNA sequencing

Immediately after completion of the electrophysiology recording, hippocampal slices were flash frozen for processing. Frozen sections were thawed in Qiazol for lysis, and total RNA was extracted using miRNeasy kit (217084) following standard protocol with on column DNase digestion (Qiagen). RNA sequencing libraries were prepared with 200 ng of total RNA using KAPA RiboErase Stranded RNA-Seq kit (KK8483) following standard protocol (Roche). Sequencing was done at Stanford Functional Genomics Facility (Stanford, CA) on an Illumina HighSeq 4000 targeting ≈ 40 million 150 bp paired-end reads per sample.

2.14 | RNA sequencing data processing pipeline

FASTQ files generated from 18 samples consisted of stimulated hippocampal slices in the following four experimental groups: WT-Veh-TBS, $n = 4$ slices; WT-BD10-2-TBS, $n = 4$ slices; APP-Veh-TBS, $n = 4$ slices; and APP-BD10-2-TBS, $n = 6$ slices. Paired-end FASTQ files were run through a unified RNA-Seq processing pipeline based on the ENCODE RNA-seq pipeline.[40,41] FASTQ files were trimmed for adapter sequences and low quality base calls (Phred < 30 at ends) using Cutadapt v1.8.1.[42] Trimmed reads were then aligned to the GRCm38.p6 (mm10) reference genome with STAR 2.7.6a[43] using gene annotations from GENCODE release vM23. Gene counts were calculated using RSEM v1.3.1.[44] Quality control metrics were calculated using featureCounts v1.6,[45] PicardTools v2.23.4,[46] and Samtools v1.11.[47]

2.15 | RNA-Seq quality control and normalization

RNA-Seq quality control and normalization expected counts were compiled from gene-level RSEM quantifications and imported into R[48] for downstream analyses. Expressed genes were defined as genes with transcript per million > 0.2 in at least 50% of samples from each group (WT-Veh-TBS, WT-BD10-2-TBS, APP-Veh-TBS, or APP-BD10-2-TBS). Only expressed genes were included in the analysis. A total of 23,407 expressed genes were used in the downstream analysis using the GENCODE M23 annotation gtf file. Principal component analysis (PCA) was calculated and plots were colored by drug treatment and genotype effect; and hierarchical clustering using Poisson distance with PoiClaClu 1.0.2.1 (Figure S1A in supporting information).[49] One sample, BD10_2_30, failed both PCA and Poisson clustering and was removed as an outlier. Outliers were defined by the majority of three analyses: Standardized sample network connectivity |Z scores| > 2, as previously described[50] (Figure S1B).

2.16 | Covariate selection

We compiled a set of 152 RNA-Seq quality control metrics from the outputs of cutadapt, STAR, featureCounts, and PicardTools (MarkDuplicates, CollectGcBiasMetrics, CollectAlignmentSummaryMetrics, CollectInsertSizeMetrics, CollectRnaSeqMetrics). These measures were summarized by the top 36 principal components, which explained the total variance of each group. Multivariate adaptive regression splines implemented in the earth package in R was used to determine which covariates to include in the final differential expression model. The potential covariates included: genotype, LTP effect, drug treatment, and seqPCs. These covariates were incorporated into

the earth model along with gene expression data. The model was run using linear predictors and otherwise default parameters. This model fits a maximum of 1000 genes simultaneously and we performed 1000 permutations randomly. None of these covariates were significant and therefore were not included in the model.

2.17 | Differential gene expression and pathway enrichment

Differential gene expression (DE) analyses was performed using DESeq2.[51] DE results with *P*adj < 0.05 were used for downstream enrichment analysis. The biomaRt v3.12[52] package in R was used to extract gene names, gene biotypes, and gene descriptions. Enrichment for Gene Ontology (GO; biological process, cellular component, and molecular function), Kyoto Encyclopedia of Genes and Genomes pathways and Reactome were performed using gprofiler2 v0.2.0.[53] Background was restricted to the expressed set of genes. Only pathways containing < 1000 genes were assessed. An ordered query was used, ranking genes by *P* value for DE analyses.

2.18 | Network co-expression analysis

Network analysis was performed with the Weighted Gene Correlation Network Analysis (version 1.70[54]) package using signed networks. A soft-threshold power of 10 was used to achieve approximate scale-free topology ($R^2 > 0.8$). The blockwiseModules function was used to construct the networks. The network dendrogram was created using average linkage hierarchical clustering of the topological overlap dissimilarity matrix (1-TOM). The hybrid dynamic tree-cutting method was used to define modules. Modules were summarized by their first principal component (ME, module eigengene) and modules with eigengene correlations > 0.9 were merged. Genes within each module were ranked based on their module membership (kME), defined as correlation to the module eigengene.

2.19 | Cell type and human-mouse co-expression module enrichment analysis

Cell type enrichment analyses were performed using several mouse-derived cell type–specific expression datasets.[55–57] Human-mouse co-expression modules from Wan et al.[58] were accessed from the Sage Bionetworks Synapse Portal (syn10309369.1), and grouped according to the reported consensus clusters and brain regions: yellow—A—astroglial-like modules; light blue—B—microglial-like modules; maroon—C—neuronal-associated modules; green—D—oligodendroglial-like modules; dark brown—E—accessory neuronal associated modules. Enrichment was performed for cell type–specific marker genes using Fisher exact test, followed by false discovery rate (FDR) correction for multiple testing. Jaccard indices and odds ratios for Fisher exact tests were generated using the GeneOverlap package (1.26.0).[59]

2.20 | Additional statistical analyses

Statistical significance was determined with GraphPad Prism software v9.01. The number of samples, mice, and measurements are included in the figure legends. Data were assessed for normal distribution and parametric or non-parametric tests were applied accordingly. Specific statistical methods for each study, including analysis of variance (ANOVA) and post hoc analyses, are specified in the figure legends.

3 | RESULTS

3.1 | BD10-2 promotes cell survival via TrkB and TrkC

Our laboratory previously identified a parent compound, LM22B-10, as a selective, small molecule activator of TrkB and TrkC that increased hippocampal cell survival and prevented dendritic spine loss in aged mice; however, it had limited blood–brain barrier penetration when given orally.[24] To improve bioavailability, a derivative of LM22B-10, designated as PTX-BD10-2 (BD10-2), was developed that achieves higher brain concentrations than the parent compound[25] (see Figure 1A for chemical structures). The specificity and trophic activity of BD10-2 was examined by assessing effects on survival of 3T3-cells expressing one of four neurotrophin receptors (TrkA, TrkB, TrkC, or $p75^{NTR}$) after treatment with BD10-2, LM22B-10, or the exogenous neurotrophins that bind to these receptors (nerve growth factor [NGF], BDNF, NT-3). The 3T3 parental cell line does not express Trk or p75 receptors and, as expected, adding BDNF or BD10-2 to serum-free medium did not support their survival (data not shown). However, 3T3 cells engineered to stably express TrkB (Figure 1B), TrkC (Figure 1C), or TrkA (Figure 1D) receptors exhibited robust survival responses to the cognate ligands BDNF, NT-3, and NGF, respectively. Cell survival was not significantly affected in BDNF-treated 3T3-p75 cells (Figure 1E). BD10-2 promoted survival of 3T3-TrkB and 3T3-TrkC cells in a dose-dependent manner and at a similar efficacy and maximal effect as the parent compound LM22B-10 and the neurotrophins BDNF and NT-3 (Figure 1B–C), but had no effect on survival of TrkA- or p75-expressing 3T3 cells (Figure 1D–E). To determine whether BD10-2 promoted survival of cultured hippocampal neurons, the number of neurons immunostained for III β-tubulin (Tuj1), a neuron-specific marker, was quantitated after exposure to BDNF, NT-3, LM22B-10, or BD10-2. The number of surviving hippocampal neurons was higher in cells treated with BDNF, NT-3, BD10-2, and LM22B-10 compared to cells in culture medium alone (Figure 1F,G). These results demonstrate that BD10-2 has survival-promoting activity with similar efficacy, although with lower potency, to that of BDNF and NT-3 and that these effects are specific to TrkB- and TrkC-expressing cells. Based on this evidence, we

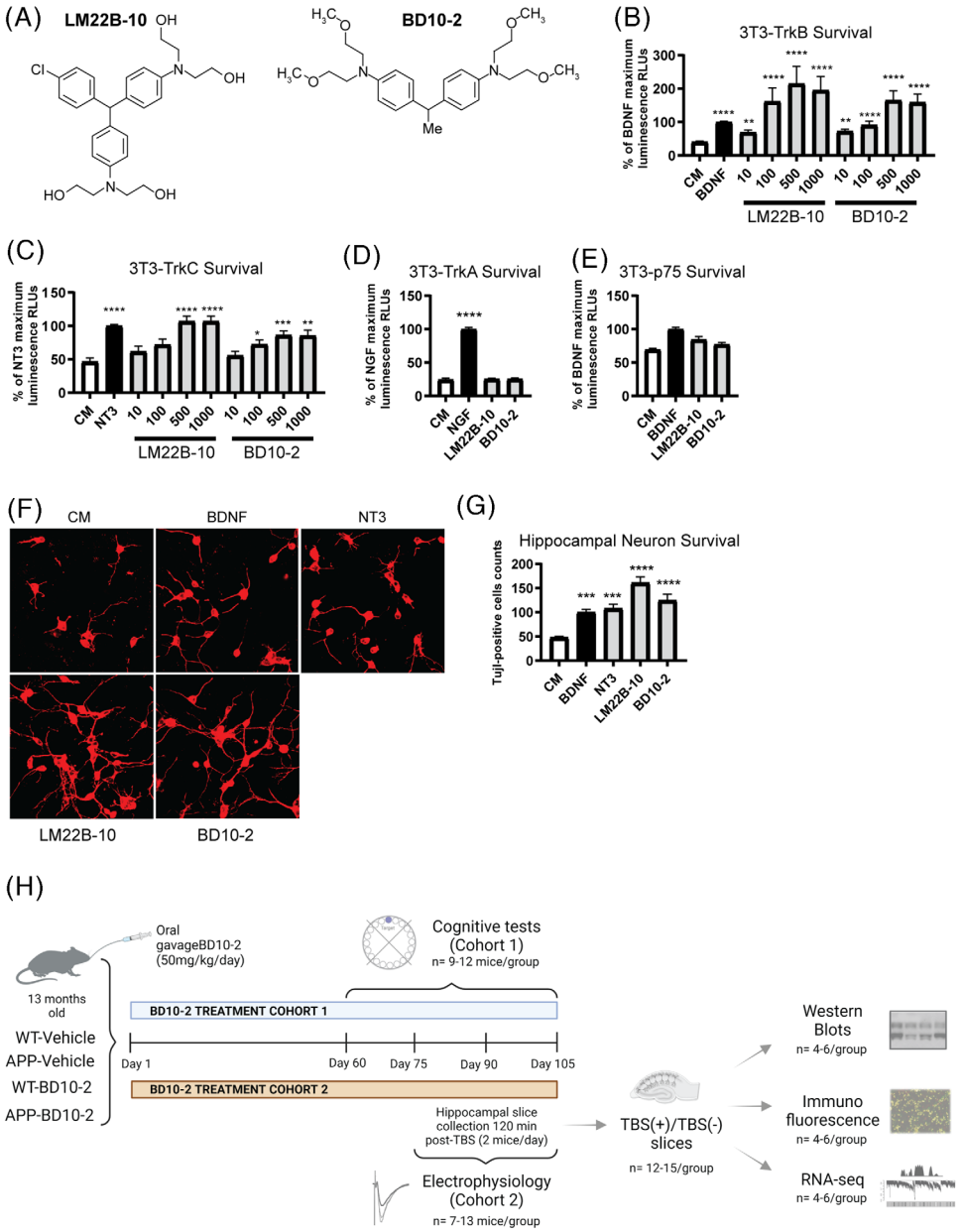

FIGURE 1 BD10-2 promotes cell survival preferentially through TrkB and TrkC. A, Structure of BD10-2 and its parent compound, LM22B-10. B–E, Trk-expressing 3T3 cells were incubated in serum-free CM alone or in CM supplemented with exogenous NTs, LM22B-10, or BD10-2 for 72 to 96 hours until survival was measured using the ViaLight assay. BD10-2 and its parent compound LM22B-10 had a dose-dependent effect on survival of (B) 3T3-TrkB, (C) 3T3-TrkC cells (mean ± SEM, $n = 16$-40 wells derived from 8–9 independent experiments). Statistical significance was determined by Kruskal–Wallis test with Dunn post hoc multiple comparison tests. $^{*}P \leq 0.05$, $^{**}P \leq 0.01$, $^{***}P \leq 0.001$, $^{****}P \leq 0.0001$ compared to CM alone. D–E, BD10-2 (1000 nM) and its parent compound LM22B-10 (1000 nM) had no effect on survival of (D) 3T3-TrkA or (E) 3T3-p75 cells compared to CM alone (mean ± SEM, $n = 24$ wells derived from four independent experiments). Statistical significance was determined by Kruskal–Wallis test with Dunn post hoc multiple comparison tests. $^{****}P \leq 0.0001$ compared to CM alone. F, BD10-2 supports the survival of cultured hippocampal neurons. Fluorescence photomicrographs (original magnification, 40×) of Tuj1-immunostained E16 mouse hippocampal neurons treated with either serum-free CM alone, BDNF, NT-3, LM22B-10, or BD10-2 for 48 hours. G, Survival analysis of hippocampal neurons treated with either BDNF (20 ng/mL), LM22B-10 (1000 nM), or BD10-2 (1000 nM) for 48 hours. Treated Tuj1-positive cells were counted and compared to wells receiving CM alone (mean ± SEM, $n = 11$ wells per group derived from three independent experiments). Statistical significance was determined by ANOVA with Dunnett post hoc multiple comparison tests. $^{***}P \leq 0.001$, $^{****}P \leq 0.0001$ compared to CM. H, Schematic representation of experimental design for in vivo experiments with chronic administration of BD10-2. ANOVA, analysis of variance; CM, culture media; BDNF, brain-derived neurotrophic factor; NT, neurotrophins; SEM, standard error of the mean; TrkB, tropomyosin related kinase B; TrkC, tropomyosin related kinase C; TBS, theta-burst stimulation; Tuj1, β-tubulin III; WT, wild type.

designed an experimental schedule to evaluate the effect of chronic treatment with BD10-2 (Figure 1H).

3.2 | Acute and chronic BD10-2 treatment reduces synaptic plasticity deficits in hippocampal slices from APP$^{L/S}$ mice at 16 months of age

BDNF activation of TrkB receptor signaling has a well-established role in promoting activity-dependent forms of synaptic plasticity such as hippocampal LTP.[60,61] Recent work has shown that NT-3/TrkC also modulates synaptic transmission.[14] We determined whether application of BD10-2 can acutely effect long-lasting changes in hippocampal synaptic plasticity. Hippocampal slices were prepared from APP$^{L/S}$ and WT mice at 16 months of age and BD10-2 (100 nM) or its Veh (HPCD) was added to the slice bath 20 minutes prior to TBS. TBS was used to induce LTP because this pattern of stimulation is based on the "hippocampal theta rhythm," a large-amplitude oscillation seen in electroencephalographic recordings in the range of 4 to 8 Hz,[62–65] and it more closely mimics in vivo physiological conditions than high-frequency stimulation, which consists of long stimulation bursts at 100 Hz.[62,66] We used a 3xTBS protocol because, compared to a single TBS protocol, it induces a stronger and longer lasting change in synaptic transmission, which allows the induction of late phases of LTP.[6] After 3xTBS, both the induction and maintenance of LTP were impaired in Veh-treated hippocampal slices from APP$^{L/S}$ mice (APP-Veh-TBS) compared to those from WTs (WT-Veh-TBS: 1 minute 190% ± 11%, 130 minutes 124% ± 7%, $n = 5$; APP-Veh-TBS: 1 minute after TBS application 152% ± 6%, 130 minutes 91% ±5%, $n = 4$; main effect of group for 2 hours post-induction: $F_{1,7} = 11.66$, $P = 0.0112$, RM-ANOVA). Bath application of BD10-2 prevented deficits in both LTP induction and maintenance in slices from APP$^{L/S}$ mice (APP-BD10-2-TBS: 1 minute 199% ± 9%, 130 minutes 128 ± 16, $n = 5$) compared to APP$^{L/S}$ slices exposed to Veh ($F_{1,7} = 7.078$, $P = 0.0325$, RM-ANOVA; Figure 2A). While the last 30 minutes of the LTP curve in WT slices treated with BD10-2 exhibited a trend toward significant potentiation compared to WT-Veh, statistical analysis revealed no significant difference between these two groups ($P > 0.05$). These data suggest that BD10-2 can restore deficits in hippocampal LTP in APP$^{L/S}$ mice and may do so through acute effects of the ligand at the TrkB/TrkC receptors.

Next, we investigated whether chronic 3-month treatment with BD10-2 would ameliorate synaptic plasticity deficits in APP$^{L/S}$ mice when the ligand was not present during recordings (Figure 1H). Hippocampal slices were prepared from mice 24 hours after they received the final dose of Veh or BD10-2, which has a plasma half-life of approximately 2 hours.[25] Basal synaptic transmission, as measured by input/output curves, via stimulation of the Schaffer collateral-CA1 pathway, was similar in hippocampal slices prepared from APP$^{L/S}$ and WT mice regardless of treatment with Veh or BD10-2 (Figure 2B). Presynaptic–mediated, short-term plasticity, and synaptic vesicle release probability was investigated using paired-pulse facilitation. PPRs were significantly decreased in APP-Veh compared to WT-Veh mice when the time between stimulation pulses was 10 ms ($P = 0.0014$), 20 ms ($P = 0.0353$), and 50 ms ($P = 0.0422$; one-way ANOVA with uncorrected Fisher least significant difference [LSD]; APP$^{L/S}$ $n = 7$ mice, WT $n = 5$ mice; Figure 2C), but not at longer inter-stimulus intervals suggesting short-term plasticity deficits. Prior BD10-2 treatment alleviated the PPR deficits in APP$^{L/S}$ mice at 10 ms ($P < 0.0001$) and 20 ms ($P = 0.0252$; one-way ANOVA with uncorrected Fisher LSD) which did not differ from WT-Veh mice at any inter-stimulus interval suggesting that TrkB/C modulation ameliorated deficits in pre-synaptic inhibitory mechanisms. As shown in acutely prepared slices in Figure 2D, LTP was also significantly impaired in hippocampal slices from chronically treated APP-Veh-TBS mice compared to WT-Veh-TBS at 16 months of age and this finding was confirmed across 120 minutes of recording (Figure 2D). The potentiated responses were significantly closer to baseline in slices from APP-Veh-TBS mice compared to WT-Veh-TBS and continued to decline over the 120 minute post-TBS interval (WT-Veh-TBS: 1 minute 180% ± 8%, 10 minutes 170% ± 6%, 120 minutes 138% ± 10%, $n = 9$; APP-Veh-TBS: 1 minute 158% ± 7%, 10 minutes 142% ± 5%, 120 minutes 111% ± 8%; $n = 9$; main genotype effect for 120 minutes recording post-TBS: $F_{1,16} = 9.695$, $P = 0.0067$, RM-ANOVA; Figure 2D). In contrast, in slices from APP$^{L/S}$ mice chronically treated with BD10-2, LTP was induced and maintained at a magnitude similar to WT-Veh-TBS and was significantly higher than APP-Veh-TBS mice at 1, 10, and 120 minutes post-TBS (APP-BD10-2: 1 minute 205% ± 14%, 10 minutes 173% ± 12%, 120 minutes 151% ± 21%; $n = 9$; APP-Veh: 1 minute 158% ± 7%, 10 minutes 142% ± 5%, 120 minutes 111% ± 8%; $n = 9$; main drug effect for 120 minutes recording post-TBS: $F_{1,16} = 7.451$, $P = 0.0148$, RM-ANOVA; Figure 2D).

3.3 | Modulation of TrkB/TrkC receptors with the small molecule ligand, BD10-2, alleviates hippocampal memory deficits in APP$^{L/S}$ mice

Given that BD10-2, when administered either acutely to brain slices, or chronically over 3 months in vivo, prevented LTP deficits and synaptic dysfunction in hippocampal slices from APP$^{L/S}$ mice, we determined whether chronic treatment with BD10-2 would reduce memory deficits in behavioral assays. WT and APP$^{L/S}$ mice were treated with BD10-2 or Veh (HPCD) by OG for 3 months beginning at 13 months of age, at which time amyloid pathology, initially evident at age 3 to 5 months, is well established in both the frontal cortex and hippocampus of APP$^{L/S}$ mice.[27,28] During the last month of BD10-2 treatment (≈ 15.5 months of age), hippocampal-dependent memory tests were performed including NOR, NOD, and Barnes maze tests to assess BD10-2's effects on cognition. The NOR test assesses recognition memory and is based on the tendency of cognitively normal rodents to spend more time exploring a novel object than a familiar one (Figure 3A). Similarly, the NOD test is based on the tendency of rodents to spend more time exploring a displaced object than one in a familiar location (Figure 3C). We found that APP$^{L/S}$ mice treated with Veh (APP-Veh) spent significantly less time with the novel object compared to WT mice treated with Veh (WT-Veh; Figure 3B). They also spent less time with the familiar object in a novel location in

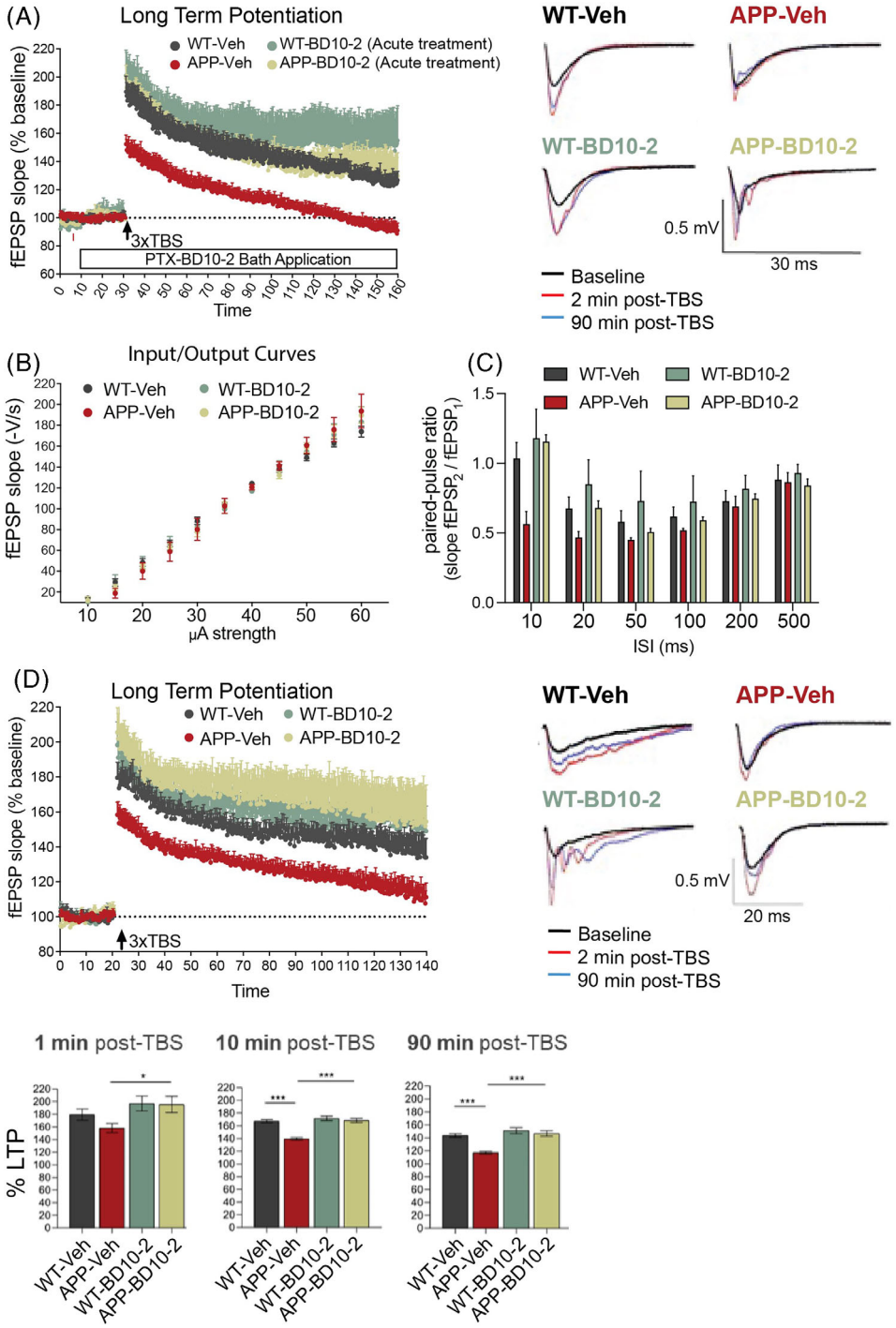

FIGURE 2 Acute and chronic BD10-2 treatment ameliorates LTP abnormalities in APP$^{L/S}$ mice. A, Hippocampal slices from APP$^{L/S}$ mice treated with Veh display significantly lower LTP magnitude both at the induction and maintenance phases compared to WT. Acute application of BD10-2 (100 nM) restored LTP in slices from APP$^{L/S}$ mice. The bar along the *x* axis indicates duration of drug application. Insets depict representative analog traces, obtained during baseline recording (black line), 2 minutes after 3xTBS (red line), and at the end of recording (130 minutes post 3xTBS; blue line) for all four groups (mean ± SEM, $n = 2–3$ mice with 4–5 slices per condition). (B)–(D) Deficits in hippocampal synaptic plasticity are ameliorated in APP$^{L/S}$ mice at 16 months of age by prior in vivo treatment with BD10-2 (mean ± SEM, $n = 6$-7 mice with 9–12 slices per condition). B, Basal synaptic transmission, as measured by input/output curves, did not differ significantly between genotypes and treatment groups. C, PPRs were decreased at the 10, 20, and 50 ms inter-pulse intervals in hippocampal slices from APP-Veh mice compared to WT-Veh ($P = 0.0014$, $P = 0.0353$, and $P = 0.0422$, respectively; one-way ANOVA with uncorrected Fisher LSD); deficits in PPRs were prevented at the 10 and 20 ms inter-pulse intervals in slices from APP-BD10-2 mice ($P < 0.0001$ and $P = 0.0252$ respectively; one-way ANOVA with uncorrected Fisher LSD). (D) *Upper panel*: The slope of fEPSPs, expressed as a percentage of baseline, showed a smaller initial amplitude in slices from APP-Veh mice than those from WT-Veh mice and decayed toward baseline indicating impaired maintenance of potentiation. Treating APP$^{L/S}$ mice with BD10-2 eliminated deficits in both the induction and maintenance of LTP. *Bottom panel*: The percentage of potentiation is reduced at 10 and 90 minutes post-TBS in hippocampal slices from APP-Veh mice ($P < 0.0001$ and $P < 0.0001$, respectively; one-way ANOVA with uncorrected

the NOD task (Figure 3D). APP$^{L/S}$ mice treated with BD10-2 (APP-BD10-2) exhibited improved ability to discriminate the novel object and location compared to APP-Veh mice (Figure 3B,D). These results demonstrate that hippocampus-dependent memory deficits observed in aged APP$^{L/S}$ mice are rescued by BD10-2.

The Barnes maze is a test of spatial learning and memory in which the mice must learn a target location using distal visual cues to escape a mildly aversive stimulus of bright light and open space (Figure 3E). After habituation (day 1) and during training (days 2 and 3), all mice learned the location of the target escape hole with a similar latency (Figure 3F). When tested 24 hours later, APP-Veh mice took longer to enter the target escape hole than WT-Veh mice (Figure 3G) and spent significantly less time in the target quadrant of the maze (Figure 3H) suggesting spatial memory impairments. Treating APP$^{L/S}$ mice with BD10-2 ameliorated the spatial memory deficits as they located the escape hole faster and spent more time in the target quadrant compared to APP-Veh mice (Figure 3G,H). These results indicate that spatial memory deficits observed in aged APP$^{L/S}$ mice are rescued by BD10-2.

3.4 | Treating APP$^{L/S}$ with BD10-2 normalizes synaptic markers and synaptic plasticity-related signaling proteins in hippocampal slices

To elucidate mechanisms by which BD10-2 ameliorates synaptic dysfunction in APP$^{L/S}$ mice, we determined whether synaptic proteins that function to maintain LTP and that are known to be affected by BDNF/TrkB or NT-3/TrkC signaling are altered in APP$^{L/S}$ hippocampal slices, and to what extent treatment with BD10-2 might affect one or more of these proteins. Hippocampal slices were collected from each group of mice that were chronically treated with Veh or BD10-2 that either received or did not receive TBS (eight treatment groups in total). To optimize the statistical power of the analyses given the number of mice studied, two to three hippocampal slices per mouse were examined, and each of these slices were considered statistically independent observations. Western blotting for the post-synaptic marker, PSD-95, or the pre-synaptic marker, synaptophysin, were performed using lysates prepared from hippocampal slices that did not receive TBS. APP-Veh mice at 16 months of age exhibited a 31% reduction in PSD-95 levels compared to WT-Veh mice; BD10-2 prevented this decrease and showed PSD-95 levels similar to WT-Veh (Figure 4A,B). BD10-2 did not affect PSD-95 levels in WT mice (Figure 4A,B). Although a previous study showed decreases in synaptophysin in the hippocampus of APP$^{L/S}$ mice at 5 to 7 months of age,[27] we observed no changes in synaptophysin (Figure 4A,C).

LTP induction is mediated, in part, by AMPAR trafficking in post-synaptic neurons.[67] AMPAR delivery to the synapse can be initiated by phosphorylation of the AMPAR GluA1 subunit by CaMKII.[68] BDNF/TrkB signaling has been implicated in this process through activation of PLCγ/PKC signaling, which activates CaMKII.[68–72] We assessed via western blotting the effects of BD10-2 on the phosphorylation and activation of kinases associated with three of the main TrkB/C signaling pathways including: CaMKII α/β (phosphorylated [p] at site Thr286), a signaling intermediate of the PLCγ/PKC pathway; Akt (Ser 473) part of the PI3K/Akt pathway; and ERK1/2 (Thr202/Tyr204 site) in the MAPK/ERK pathway. Activation of each of these pathways has been shown to be disrupted in AD mice contributing to LTP deficits.[73–79] First, we assessed whether activation, as indicated by phosphorylation of selected signaling proteins within these pathways, was affected in APP$^{L/S}$ mice under baseline conditions (TBS–) and, if so, whether BD10-2 normalizes these changes. Activity levels, as indicated by the ratio of pCaMKIIα, pCaMKIIβ, and pAkt over respective total protein, were significantly decreased in slices from APP-Veh mice compared to WT-Veh slices (Figure 4A,D–F), while the ratio of pERK was unchanged (Figure 4A,G). Chronic treatment with BD10-2 normalized pCaMKIIβ and pAkt ratios in APP hippocampal slices (Figure 4A,E,F), but not pCaMKIIα (Figure 4A,D) or pERK ratios (Figure 4A,G). Phosphorylation of CaMKIIα, CaMKIIβ, Akt, and ERK were unchanged in WT-BD10-2 mice compared to that from WT-Veh mice (Figure 4A,D–G). Total protein levels, as indicated by ratio of protein over actin, of each of these signaling molecules did not differ between any of the treatment groups (Figure 4A, S2A–D in supporting information). Because CaMKII can phosphorylate GluA1 and thereby regulate its delivery to the synapse,[72,80] we assessed the effects of BD10-2 on GluA1 phosphorylation at Ser831 (pGluA1), a site phosphorylated by CaMKII.[81] The ratio of pGluA1/GluA was reduced in hippocampal slices from APP-Veh mice compared to WT-Veh while BD10-2 prevented this decrease. The ratio pGluA1/GluA1 did not change in WT mice in response to BD10-2 treatment (Figure 4A,H) and total protein levels of GluA1 remained stable in all treatment conditions (Figure 4A, S2E).

Because we observed changes in baseline activation of proteins associated with LTP that were normalized by BD10-2, we asked whether the same would be true in hippocampal slices that underwent TBS (TBS+). Like unstimulated hippocampi, TBS+ slices from APP-Veh mice showed reductions in PSD-95 and pAkt/Akt compared to WT-Veh mice; however, BD10-2 had no effect on these deficits (Figure S2F, G, M). Notably, pGluA1/GluA1 was also reduced in TBS+ hippocampal slices from APP$^{L/S}$ mice compared to WT-Veh; BD10-2 prevented this decrease (Figure 4I,J). No changes in any of the other activation ratios or protein levels examined in the unstimulated slices were seen between any of the treatment groups in TBS+ slices (Figure S2F,H–L, N-Q). The modest degree of statistical significance in the present western blot signaling data will encourage additional investigation using increased sample sizes and

Fisher LSD) and back to WT level in slices from APP$^{L/S}$ mice after in vivo treatment with BD10-2 at 1, 10, and 90 minutes post TBS ($P = 0.0204$, $P < 0.0001$, and $P < 0.0001$; one-way ANOVA with uncorrected Fisher LSD). ANOVA, analysis of variance; fEPSPs, field excitatory post-synaptic potentials; LSD, least significant difference; LTP, long-term potentiation; PPR, paired-pulse ratio; SEM, standard error of the mean; TBS, theta-burst stimulation; Veh, vehicle; WT, wild type.

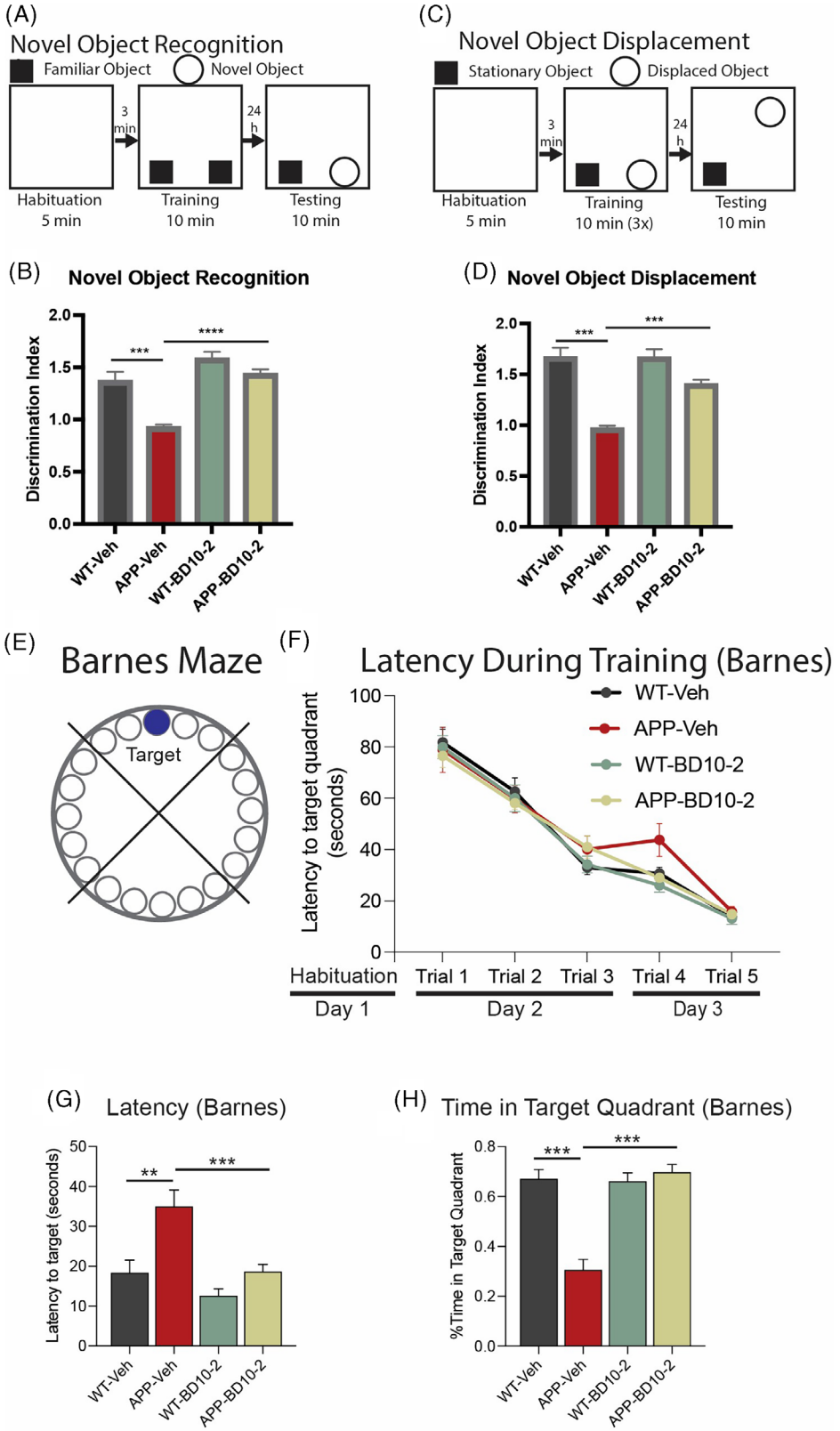

FIGURE 3 Long-term treatment with BD10-2 ameliorates cognitive abnormalities in aged APP$^{L/S}$ mice. A–H, Behavioral tests of cognition in APP$^{L/S}$ mice treated with BD10-2 by oral gavage for 3 months starting at 13 months of age (mean ± SEM, $n = 9–12$ mice per group). A, For the NOR test, mice were habituated to an arena for 5 minutes prior to the training session where two identical objects were placed in the arena and the mice were allowed to explore for 10 minutes. After 24 hours, mice were returned to the arena in which one of the familiar objects was replaced by a novel object and exploratory behavior around the objects was tracked for 10 minutes. B, In the NOR test, APP-Veh mice showed prominent deficits in discriminating between novel and familiar objects compared to WT-Veh ($P < 0.0001$; one-way ANOVA with uncorrected Fisher LSD); BD10-2 treatment prevented this deficit ($P < 0.0001$; one-way ANOVA with uncorrected Fisher LSD). C, For the NOD test mice were habituated to an

additional measures to further assess the generalizability of our results.

Given that BD10-2 normalized pGluA1 levels in both stimulated and unstimulated hippocampal slices of APP$^{L/S}$ mice and GluA1 phosphorylation is associated with AMPAR transport to the synapse, we assessed whether chronic BD10-2 treatment increased levels of GluA1 in synapses within the CA1 region of hippocampal slices from APP$^{L/S}$ and WT mice with and without TBS. Synaptic localization was evaluated using the colocalization of immunostaining for GluA1 and the post-synaptic marker, drebrin. To compare the effects of stimulation, genotype, and BD10-2, data were normalized to the WT-Veh condition without TBS. At baseline conditions (without TBS), the amount of GluA1 colocalized with drebrin (M1 Mander coefficient) was significantly decreased in hippocampal slices from APP-Veh compared to WT-Veh mice; BD10-2 did not change colocalization in unstimulated slices (Figure 4K,L). GluA1 colocalization with drebrin was increased in WT-Veh slices 2 hours post-TBS compared to unstimulated slices from WT-Veh mice. In contrast, TBS failed to increase GluA1-drebrin colocalization in APP-Veh slices compared to unstimulated APP-Veh slices (Figure 4K,L). Similar to the unstimulated condition, GluA1-drebrin colocalization was reduced in slices from stimulated APP-Veh slices compared to stimulated WT-Veh slices. Interestingly, in contrast to unstimulated slices, BD10-2 partially rescued GluA1-drebrin colocalization in stimulated hippocampal slices from APP$^{L/S}$ mice (Figure 4K,L), suggesting that one mechanism by which BD10-2 might alleviate LTP deficits is by enhancing localization of GluA1-AMPARs to synapses.

3.5 | Chronic treatment with BD10-2 restores the number of excitatory synapses in hippocampal slices despite no changes in Aβ plaque load

Studies have shown that AD brains exhibit a loss of excitatory synapses, primarily in the hippocampus,[2] contributing to impaired neuronal communication and network activity, ultimately leading to cognitive decline.[82–84] Given the potential of enhancing excitatory synaptic function for improving cognitive function in AD, including promoting new synapse formation and protecting existing ones from degeneration, we investigated whether chronic BD10-2 treatment could restore the ability of LTP to facilitate the formation of new excitatory synapses, thereby maintaining healthy synaptic function. BD10-2 treatment significantly increased the number of excitatory synapses in hippocampal slices from APP$^{L/S}$ mice compared to controls. Immunofluorescence staining for VGlut1 (presynaptic marker) and PSD-95 (post-synaptic marker) showed reduced co-localization in APP$^{L/S}$ mice compared to WT controls (Figure 5A), suggesting a decrease in the number of functional excitatory synapses in the APP group. Notably, BD10-2 treatment for 3 months significantly increased the co-localization of VGlut1 and PSD-95 in APP$^{L/S}$ mice compared to Veh-treated controls (Figure 5A, and 5B), indicating a restoration of the excitatory synapse number in the APP-BD10-2 group.

We investigated whether the effects of BD10-2 on synaptic efficacy and protein expression seen here in APP$^{L/S}$ mice could be due in part to reductions in Aβ deposition because lowering Aβ toxicity has been hypothesized to improve synaptic function and promote the expression of synaptic proteins.[85] Therefore, we assessed the effects of BD10-2 on Aβ pathology in the hippocampal slices used for electrophysiology. Quantitative analysis of Thioflavin S staining revealed that chronic treatment with BD10-2 (from 13 to 16 months of age) did not significantly alter the percent area occupied by Aβ plaques in the hippocampal slices of APP-Veh compared to APP-BD10-2 mice (Figure 5A–D).

These findings suggest that while BD10-2 does not directly affect Aβ plaque load, it can restore the number of excitatory synapses in the hippocampus of APP$^{L/S}$ mice, potentially contributing to improved cognitive function.

3.6 | Altered activity-dependent transcriptional signatures observed in APP$^{L/S}$ mice are normalized by BD10-2 treatment

Synaptic activity-dependent transcription is critical for stabilizing the long-lasting changes established in late phase LTP (L-LTP), which requires the synthesis of new proteins implying a transcriptional shift at some point during potentiation.[5,86–94] We examined whether TBS-driven LTP affects gene transcription in WT and APP$^{L/S}$ mice and if the

arena for 5 minutes followed by three training sessions in which two identical objects were placed in the arena and the mice were allowed to explore for 10 minutes. After 24 hours, one of the objects used during training was moved to a new location and mice were returned to the arena. Exploratory behavior around the objects was tracked for 10 minutes. D, In the NOD test, the ability of APP-Veh mice to discriminate a familiar object in a novel location was impaired versus WT ($P < 0.0001$; one-way ANOVA with uncorrected Fisher LSD); this impairment was ameliorated by BD10-2 treatment ($P < 0.0001$; one-way ANOVA with uncorrected Fisher LSD). E–H, Barnes maze task: (E) the Barnes maze measures spatial memory by testing a rodent's ability to remember the location of a hole which allows them to escape mildly aversive stimuli of bright light and open space. The time spent in the target quadrant of the maze and the latency to reach the escape hole were measured. F, During training (days 2 and 3), all mice learned the location of the target quadrant and escape hole as evidenced by similar latencies to the target quadrant. G, On the test day 4, the latency to reach the target escape hole is increased in APP-Veh mice ($P = 0.0003$; one-way ANOVA with uncorrected Fisher LSD), while APP-BD10-2 mice found the target significantly faster than APP-Veh mice ($P = 0.0002$; one-way ANOVA with uncorrected Fisher LSD). H, Inversely, the percentage of time spent in the target quadrant is reduced in APP-Veh mice versus WT-Veh ($P < 0.0001$; one-way ANOVA with uncorrected Fisher LSD); treatment of APP$^{L/S}$ mice with BD10-2 prevented this deficit ($P < 0.0001$; one-way ANOVA with uncorrected Fisher LSD). ANOVA, analysis of variance; LSD, least significant difference; NOD, novel object displacement; NOR, novel object recognition; SEM, standard error of the mean; Veh, vehicle; WT, wild type.

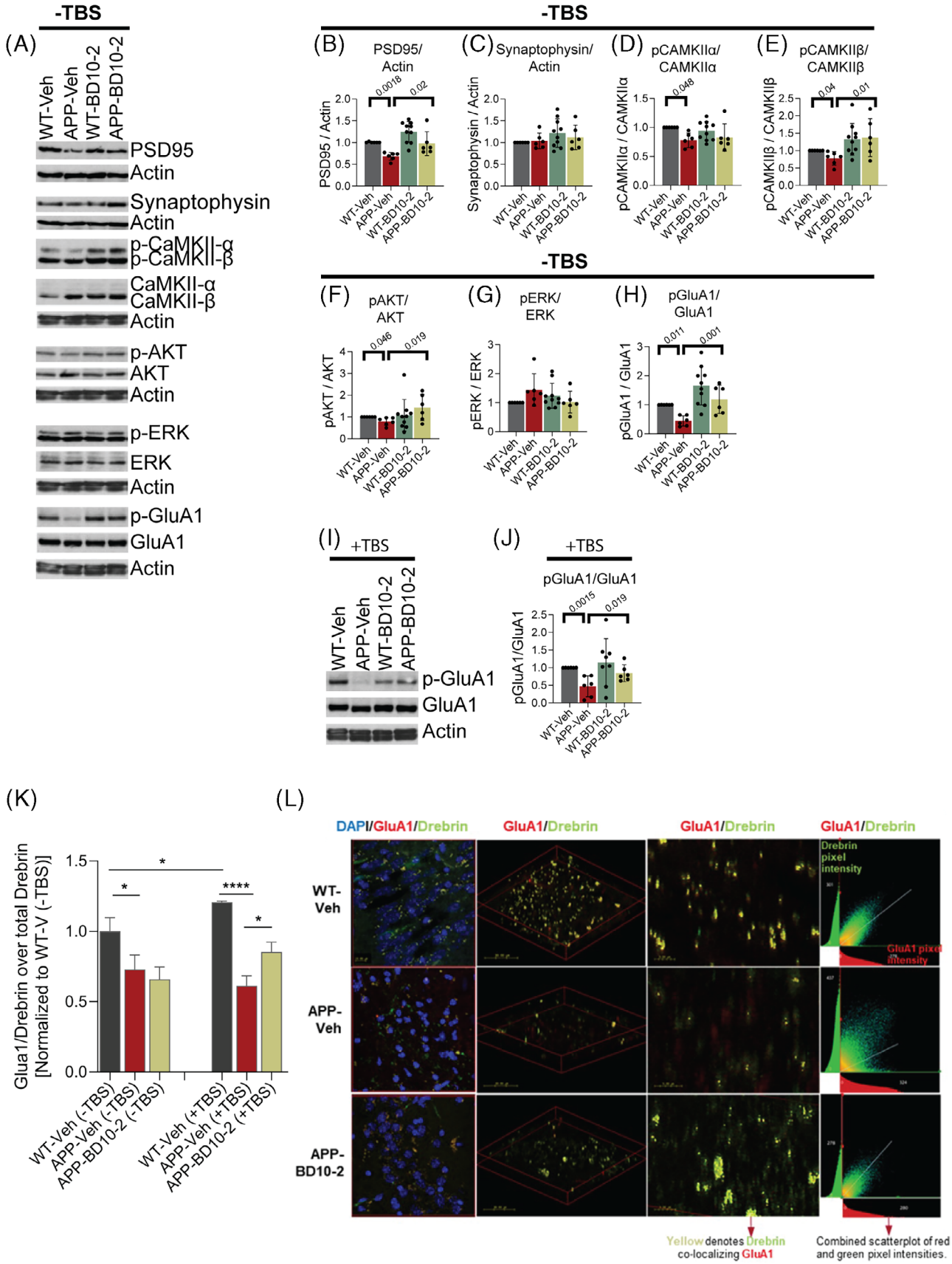

FIGURE 4 BD10-2 enhances baseline CaMKII, GluA1, and Akt phosphorylation as well as co-localization of GluA1 and drebrin in slices that underwent LTP. BD10-2 or vehicle was administered by oral gavage to 13-month-old $APP^{L/S}$ mice for 3 months, followed by collection of hippocampal slices. A, Representative western blots of unstimulated (TBS−) hippocampal slices. B–H, J, Western blots of hippocampal slice extracts were quantitated by determining the ratios of phospho (p) protein over total protein or total protein over actin, and then normalized to

restorative effects of BD10-2 on LTP in $APP^{L/S}$ mice were associated with L-LTP–related transcriptional changes. To this end, RNA sequencing was performed on hippocampal slices from WT and $APP^{L/S}$ mice that were chronically treated with BD10-2 or Veh and used for the LTP experiments in Figure 2D. A principal component analysis of the whole transcriptome revealed a strong genotype and TBS effect as there was a clear separation between their respective principal component groupings (Figure 6A) and volcano plots (Figure S3A–B in supporting information). To identify L-LTP–associated gene expression, we examined the effects of TBS on DE ($Padj < 0.05$) for groups that exhibited LTP (WT-Veh-TBS vs. WT-Veh; APP-BD10-2-TBS vs. APP-BD10-2) or impaired LTP (APP-Veh-TBS vs. APP-Veh; Figure 6B–D, Tables S1–S7 in supporting information). Genes that changed with TBS in WT-Veh mice, which exhibited LTP, and APP-Veh mice, which did not, can be classified by quadrant. The *y* axis shows the difference in TBS gene expression between WT-Veh and APP-Veh mice, with opposing direction of fold change indicating those associated with LTP (Figure 6B). Quadrants 1 and 4 show genes that are upregulated with TBS in WT mice. Both show strong general immune-associated GO enrichment (Table S7). Quadrant 4 gene enrichments represent those lessened or lost in the APP-Veh-TBS mice; these include cytokines, and genes involved in apoptosis and MAPK signaling. Genes in quadrant 2 are downregulated with TBS in WT-Veh mice and are increased or upregulated with TBS in APP-Veh mice. Quadrant 2 genes show relevance to synaptic function, signaling, angiogenesis, and neuron projection morphogenesis. Taken together, these data suggest that activity-dependent LTP associated transcriptional changes involve synaptic and immune processes. Additionally, the similarity in transcription patterns between the two groups that exhibited activity-dependent LTP after TBS (WT-Veh and APP-BD10-2; Figure 6), supports the hypothesis that BD10-2 reduces alterations in activity-dependent LTP associated gene expression in $APP^{L/S}$ mice.

To further explore these LTP-associated biological processes, we examined the top GO processes associated with genes that were upregulated or downregulated with TBS across the three experimental groups: WT-Veh, APP-Veh, APP-BD10-2 (Figure 6C, Tables S4–S6). Looking at the top-enriched processes in downregulated genes, GO pathways associated with synapse-related processes such as "synaptic signaling," "synapse organization," and "signal release from synapse" show a notable activity-dependent pattern. This TBS-associated downregulation only occurred in the groups demonstrating LTP (WT-Veh-TBS and APP-BD10-2-TBS) and was absent in APP-Veh slices which exhibited impaired LTP (Figure 6C). Examining the top GO processes enriched in genes upregulated by TBS showed that immune system processes were represented across all groups. Many immune-related genes were upregulated with TBS in WT-Veh mice; however, the magnitude of enrichment was greater in both APP-Veh and APP-BD10-2 groups. This result may reflect an upregulated immune response to amyloid pathology in APP-Veh that is not addressed by BD10-2 treatment.

The relevance of the effect of TBS on gene expression in AD mice to human AD was examined by performing an overlap enrichment analysis between DE genes associated with TBS in our mouse study ($Padj < 0.05$) and an AD-related human-mouse co-expression module study by Wan et al.[58] Wan's group examined consensus modules of genes that are altered in brains of human AD patients (versus non-AD controls) across multiple studies (Religious Orders Study Rush Memory and Aging Project,[95] Mount Sinai School of Medicine,[96] and Mayo[97]) and brain regions gathered by the Accelerating Medicines Partnership-Alzheimer's Disease Consortium. These co-expression modules share sizeable overlap with a broad range of mouse models of AD (251 DE gene sets), providing strong evidence they contain cross-species AD-associated genes. The modules largely group into consensus clusters that correlate to cell types. By comparing these clusters to our DE gene sets ($Padj < 0.05$), we determined which AD-related modules might be enriched in genes that are differentially expressed after TBS. The analysis demonstrated significant overlap enrichment of AD-relevant neuronal modules with genes that were downregulated by TBS in both WT and APP-BD10-2 mice but showed notably reduced enrichment in both overlap size and significance in the APP group (Figure 6D, Figure S4A in supporting information), consistent with activity-dependent LTP-associated enrichment. In contrast, microglial consensus clusters, which correspond to immune-associated processes, showed consistent enrichment of genes upregulated by TBS across all treatment groups with slightly higher enrichment in both APP-Veh and APP-BD10-2, similar to Figure 6C. This suggests that upregulation of this microglial module is relevant to amyloid model mice and human AD but occurs regardless of whether samples exhibited activity-dependent LTP.[98] Oligodendroglial and astroglial modules demonstrated a low level of enrichment after TBS and showed little evidence for

respective WT-Veh groups. Statistical significance was determined using either one way ANOVA with Sidak post hoc test or Kruskal–Wallis test with post hoc Dunn multiple comparisons test (mean ± SEM, sample size = 6–10 hippocampal slices, 3–5 mice per group, with two independent western blots averaged per slice). B–H, Quantification of unstimulated (TBS–) hippocampal slices shown in A. I, Representative western blot for hippocampal slices that underwent 3xTBS. J, Quantification of stimulated (TBS+) hippocampal slices shown in (I). K–L, Immunofluorescence staining analysis of co-localization between GluA1 and drebrin in slices that underwent 3xTBS. K, Mander's coefficient (M1) for samples stained with GluA1 and drebrin. All samples are normalized to WT-Veh without TBS. Proportion of GluA1 colocalized with drebrin in APP and WT mouse hippocampal slices without and with stimulation (mean ± SEM, $n = 3$ mice per group). $^{*}P < 0.05$; $^{****}P < 0.0001$ by uncorrected Fisher LSD multiple comparison after one-way ANOVA. L, Representative 63× confocal microscope z-stack images of stained DAPI cells and colocalized drebin and GluA1 (yellow) from different angles in slices that underwent 3xTBS. The CA1 region of the hippocampus was photographed with 0.3 µm step size to create a composite image of each slice. Middle panel demonstrates decreased colocalization in the APP vehicle mouse compared to the WT vehicle and the transgenic drug condition. Lower middle panel demonstrates increased colocalization for the $APP^{L/S}$ mouse treated for 3 months with BD10-2 compared to the untreated $APP^{L/S}$ mouse. ANOVA, analysis of variance; LTP, long-term potentiation; SEM, standard error of the mean; TBS, theta-burst stimulation; Veh, vehicle; WT, wild type.

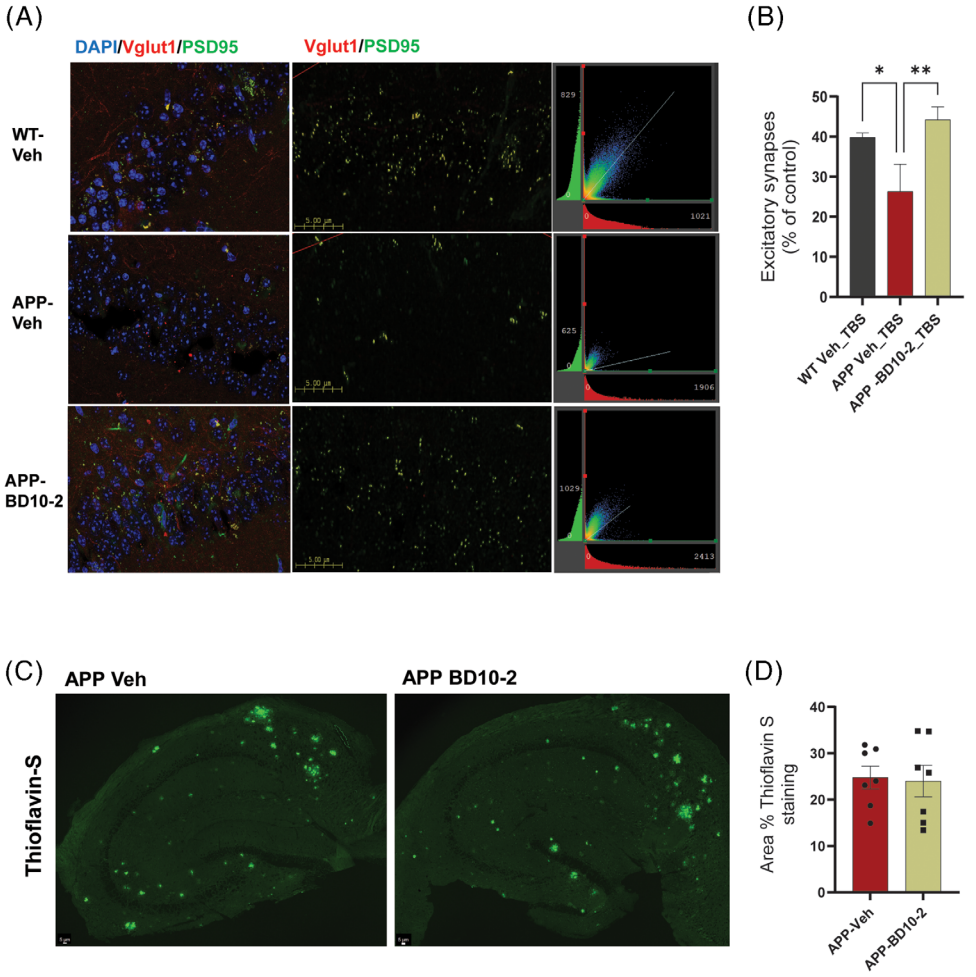

FIGURE 5 BD10-2 treatment from 13 to 16 months of age does not reduce Aβ plaque burden in the hippocampus but it increases the number of excitatory synapses in APP mice. A, Representative 63× confocal microscope z-stack images of stained DAPI cells (blue) and excitatory synapses identified by co-localization (yellow) between VGlut1 (red) and PSD-95 (green) in slices that underwent 3xTBS. The CA1 region of the hippocampus was imaged using a 0.3 µm step size to generate a composite image of each slice. In the middle panel, reduced colocalization is observed in the APP vehicle mouse compared to the WT vehicle and the transgenic drug condition. Increased colocalization is evident in the APP mouse treated with BD10-2 for 3 months compared to the untreated APP mouse. In the right panel, 2D histograms shows the relationship of VGlut1 and PSD-95 intensities concentrated along the y = x line, indicating a similar degree of overlapped signals in both the WT and APP-BD10-2 groups compared to APP group. B, Spearman coefficient for samples stained with VGlut1 and PSD-95. Percentage of colocalized VGlut1 with PSD-95 in WT, APP, and APP-BD10-2 mouse hippocampal slices with 3xTBS (mean ± SEM, n = 3 mice, 7-12 slices per group). *P < 0.05; **P < 0.005 by uncorrected Fisher LSD multiple comparison after one-way ANOVA. Aβ, amyloid beta; ANOVA, analysis of variance; SEM, standard error of the mean; TBS, theta-burst stimulation; WT, wild type. C, Representative confocal microscope images of brain slices from APP and APP-BD10-2 stained with a thioflavin S dye. D, Thioflavin S-positive percentage area was quantified indicating no difference between the two groups tested. Data are shown as ± SEM, n = 3 mice, 7 slices per group.

module-level activity-dependent enrichment. Noting that L-LTP transcriptional effects are measured 130 minutes (during late- rather than early-stage LTP) after the initiation of TBS, the data presented in Figure 6 highlight that TBS alters transcription of immune, microglial, and synaptic/neuronal processes. Perhaps unexpectedly, downregulation of synaptic/neuronal processes—rather than upregulation—is consistently specific to the LTP groups, demonstrating the strongest transcriptional signature of activity-dependent LTP, which is rescued in APP$^{L/S}$ mice with the addition of BD10-2. While broad categories of immune/microglial processes did not show clear association with activity-dependent LTP, some immune-associated genes did, suggesting more nuanced modulation of immune-associated gene expression by BD10-2 may play a role in LTP rescue.

3.7 | BD10-2 affects genes related to synaptic plasticity, neurotrophin signaling, immune responses, microglia, and oligodendrocyte function in stimulated hippocampal slices from APP$^{L/S}$ mice

After examining DE effects caused by TBS in the experimental groups, we asked whether any DE effects are driven by APP$^{L/S}$ genotype

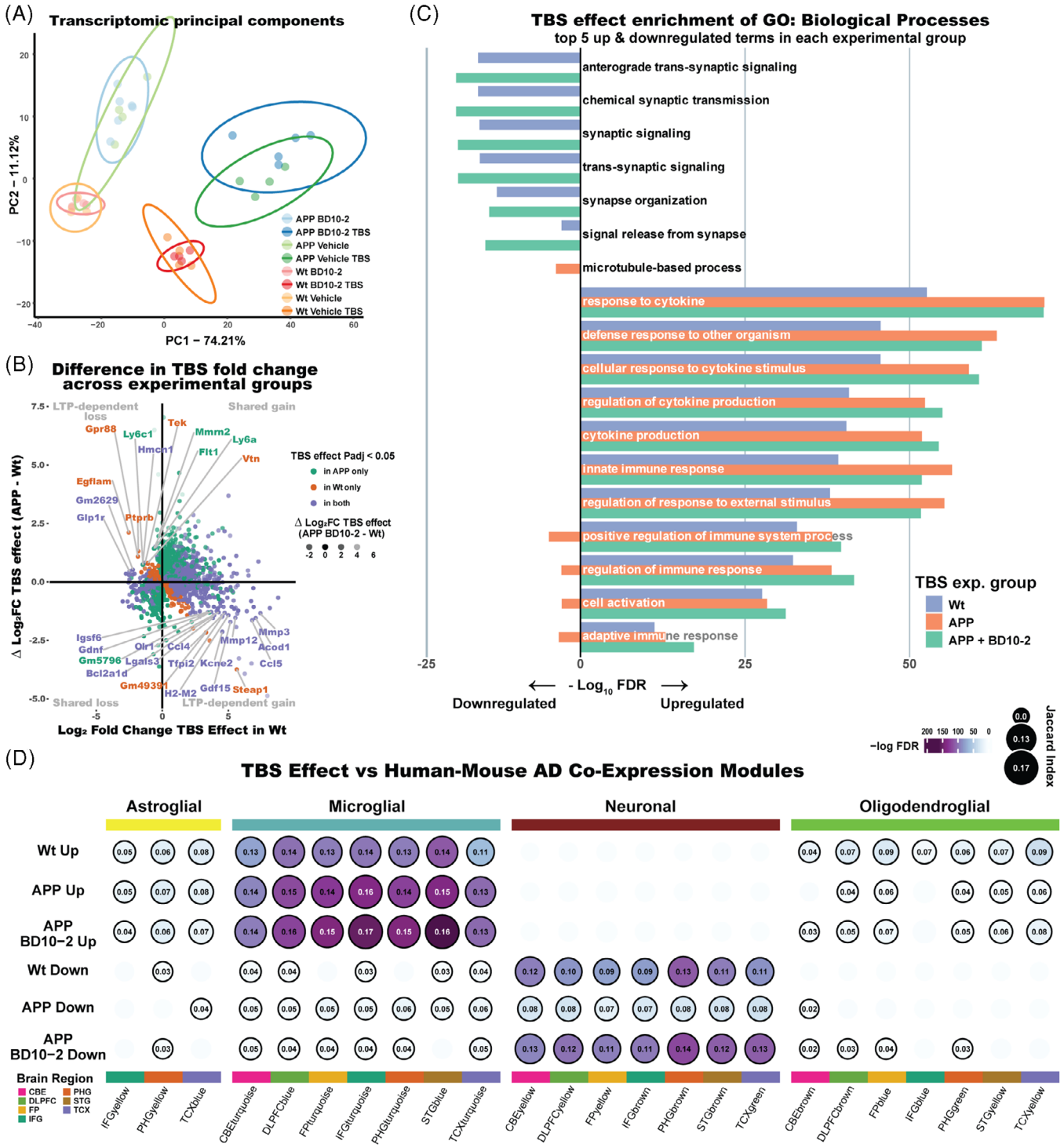

FIGURE 6 TBS causes activity-dependent transcriptional changes in WT mice that are absent in $APP^{L/S}$ mice and rescued by BD10-2 treatment. A, Principal component analysis of the top 1000 most variable genes in hippocampal slices from mice in each of the eight treatment groups: WT-Veh (orange), WT-BD10-2 (red), APP-Veh (green), APP-BD10-2 (blue) either with TBS (darker shade) or sham TBS (lighter shade). B, DE fold change comparison between TBS effects in the three treatment groups: WT-Veh (WT-Veh-TBS vs. WT-Veh), APP-Veh (APP-Veh-TBS vs. APP-Veh), and APP-BD10-2 (APP-BD10-2-TBS vs. APP-BD10-2). Genes shown are limited to those significantly DE (*Padj* < 0.05) in both WT-Veh and APP-BD10-2 together (those displaying normal LTP) or APP-Veh (which failed to induce and maintain LTP). The *x* axis depicts TBS effect in WT-Veh group, while the *y* axis shows the difference in $\log_2$ fold change between APP-Veh and WT-Veh groups, indicating LTP-relevant discordance in TBS expression. Genes significant (*Padj* < 0.05) in respective groups (or their overlap) are color coded. Spot transparency is graded by the difference in $\log_2$ fold change between WT-Veh and APP-BD10-2 groups, indicating discordance in TBS expression between the two groups that display intact LTP. C, Gene Ontology enrichment showing the effect of TBS in the three treatment groups. Up- or downregulated genes (*Padj* < 0.05) for TBS in each group was tested for enrichment of GO: Biological Process, and the top five terms for each directional set in each group were merged into 18 total terms. D, Overlap enrichment (Fisher exact) of AD-related human-mouse co-expression modules from Wan et al.[58] compared

and whether BD10-2 can ameliorate these effects among stimulated samples. Our goal was to identify changes that might influence BD10-2 mediated rescue of LTP deficits in $APP^{L/S}$ mice described above. To answer this, we asked three questions that can be answered by comparing three DE effect groups. First, how does gene expression change in $APP^{L/S}$ mice compared to WT mice (APP effect: APP-Veh-TBS vs. WT-Veh-TBS mice)? Second, how does gene expression change in BD10-2 treated $APP^{L/S}$ mice compared to untreated $APP^{L/S}$ mice (BD10-2 effect: APP-BD10-2-TBS vs. APP-Veh-TBS mice)? And third, does BD10-2 treatment restore gene expression in $APP^{L/S}$ mice to a more WT-like state (APP-BD10-2 effect: APP-BD10-2-TBS vs. WT-Veh-TBS mice)? It is important to note that the APP and APP-BD10-2 effects are normalized to the same baseline group (WT-Veh-TBS) allowing relative comparison of the effects of APP genotype alone compared to the restorative effects of BD10-2 on $APP^{L/S}$ mice in both overlap expression analysis and gene network module analysis. If BD10-2 restores $APP^{L/S}$ transcription to resemble WT-Veh transcription, there should be relatively few DE genes in the APP-BD10-2 effect. We can compare the APP effect to the APP-BD10-2 effect to observe pathway alterations between APP-Veh-TBS mice, which do not exhibit LTP, and APP-BD10-2-TBS mice, which do exhibit LTP.

In terms of principal components (Figure 6A), shifts related to BD10-2 were much smaller than those due to APP genotype or TBS; this is unsurprising given the last dose was administered > 24 hours prior to brain harvesting. The largest BD10-2–mediated DE effect observed was in the APP-TBS mice (BD10-2 effect): (APP-BD10-2-TBS [dark blue] vs. APP-Veh-TBS [dark green]; Figure 6A). However, this BD10-2 effect was smaller than either group's within-group variance, limiting our statistical power to measure these changes confidently. Accordingly, only eight genes exhibited a BD10-2 DE effect after multiple testing correction (Padj < 0.05) compared to 1384 significant DE genes associated with the APP effect and 2858 DE genes in the APP-BD10-2 effect (Figure 6A, 7A, Figure S3A–B, Tables S8–S10 in supporting information). The top significant DE genes in the BD10-2 effect include several complement pathway specific genes (*C3*, Padj < 0.02; *C1qa*, Padj < 0.14), *Kank1* (Padj < 0.009), an actin polymerization regulator and modulator of apoptotic mechanisms and axonal function,[99,100] a pair of Annexins (*Anxa2*, Padj < 0.02; *Anxa8*, Padj < 0.05), and genes associated with motility and neurite growth including *Hydin* (Padj < 0.06) and axonemal dynein (*Dnah11*, Padj < 0.005;[101] Figure 7A, Figure S3B).

Many of the top upregulated genes in the APP effect were further upregulated in the APP-BD10-2 effect, and in a few cases (e.g., *C1qa*) appeared upregulated in the BD10-2 effect as well (Figure 7A). Setting a relaxed significance threshold (P value < 0.05), we compared the fold change of DE for the APP effect (*y* axis) and BD10-2 effect (*x* axis) to gauge the correlation of genes nominally significant in both (379 genes; Figure 7B). This revealed many genes in quadrant 1 that are upregulated by both effects. Quadrant 1 is enriched for inflammatory response and cytokine production (Table S11 in supporting information). Quadrant 4 contained genes that show inverse correlation of APP and BD10-2 effects: downregulated in $APP^{L/S}$ mice and upregulated with BD10-2 treatment. Quadrant 4 was enriched for microtubule-based processes axoneme, and cilium processes. Quadrant 3 contained genes that are downregulated in both APP and BD10-2 effects and had few genes but some significant enrichment for anion transport/signaling. Although few genes were shared between APP and BD10-2 effects, we observed a notable concordance of upregulated inflammation and downregulated synaptic function-related signaling pathways.

Next, we examined selected LTP-relevant pathways including synaptic function, neurotrophin-modulated signaling, and immune terms informed by our analysis of DE effects caused by TBS. A pathway enrichment analysis was performed on APP, BD10-2, and APP-BD10-2 effects (Figure 7C, Tables S12–S14 in supporting information). A relaxed P value threshold of nominally significant genes (P < 0.05) for all groups in this comparison was applied to be able to observe BD10-2 effect changes for comparison. For most pathways, enrichment associated with the BD10-2 effect was small and often in the same direction as the APP and APP-BD10-2 effects. Notably the axoneme pathway, which contains several motility and cytoskeletal genes, was one of the few pathways where enrichment associated with the APP effect was directly opposed by a pronounced BD10-2 effect, and where no enrichment was observed in APP-BD10-2 agreeing with the correlation in individual genes in quadrant 4 of Figure 7B (Figure 7C, Tables S12–S14).

In LTP-relevant enriched terms across synapse, signaling, and potentiation, the APP-BD10-2 effect showed a much larger enrichment in downregulated genes than APP alone (Figure 7C, Tables S12–S14), consistent with the activity-dependent LTP associated downregulation seen in Figure 6. Wnt, Erk, and PI3K-Akt pathways are downstream of TrkB and TrkC signaling and are thought to be candidate mechanisms for neurotrophin modulation of synaptic plasticity.[102–104] The Wnt pathway showed enrichment in the APP effect with further enrichment in the APP-BD10-2 effect and includes *Kank1*, significant for BD10-2 effect (Padj < 0.009; Figure 7A,C, Figure S5 in supporting information, Table S9). The Erk1/2 cascade showed an interesting shift in regulation, with negative regulation being more highly enriched in the

to upregulated (top three rows)/downregulated (bottom three rows) genes in the TBS effect in the three treatment groups (Padj < 0.05). Circles are sized and annotated with the Jaccard index of their overlap and are colored by the significance of the overlap enrichment (−log FDR; circles with an FDR < 0.05 have a bold edge). Modules are grouped based on "consensus clusters": yellow, astroglial-like modules; light blue, microglial-like modules; maroon, neuronal-associated modules; green, oligodendroglial-like modules. Modules are additionally annotated along the bottom by the associated brain region of the human AD cohort from which they were derived. AD, Alzheimer's disease; CBE, cerebellum; DE, differential gene expression; DLPFC, dorsolateral prefrontal cortex; FDR, false discovery rate; FP, frontal pole; IFG, inferior frontal gyrus; LTP, long-term potentiation; PHG, parahippocampal gyrus; STG, superior temporal gyrus; TBS, theta-burst stimulation; TCX, temporal cortex; Veh, vehicle; WT, wild type.

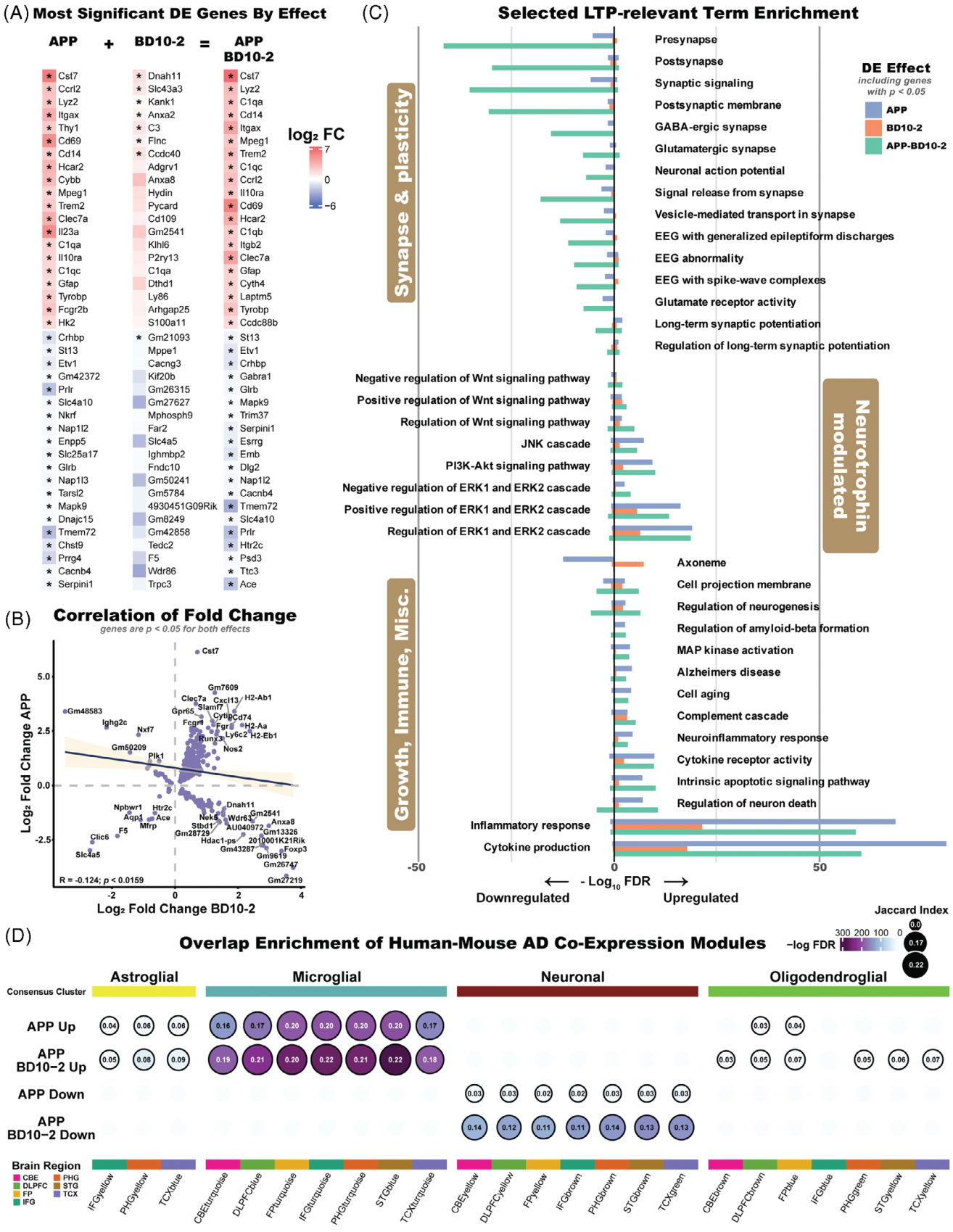

FIGURE 7 In vivo treatment of 16-month-old APP$^{L/S}$ and WT mice with BD10-2 causes transcriptomic changes in post-TBS hippocampal slices. A, The top 20 upregulated and downregulated DE genes ranked by FDR adjusted *P*-value in each of three DE comparisons: the APP effect (APP-Veh-TBS vs. WT-Veh-TBS), the BD10-2 effect (APP-BD10-2-TBS vs. APP-Veh-TBS), and the APP-BD10-2 effect (APP-BD10-2-TBS vs. WT-Veh-TBS). Colored by their $\log_2$ fold change expression, genes with an asterisk have *Padj* < 0.05 significance. B, A correlation of fold change

APP-BD10-2 effect and positive regulation more highly enriched in the APP effect. The PI3K/Akt pathway was enriched in both APP and APP-BD10-2 effect, with only modestly higher enrichment in the second, while JNK cascade showed a mild decreased enrichment in APP-BD10-2 upregulated genes compared to APP. Looking at normalized expression of these pathways (Figure S5), the trend for many genes fits a compensatory pattern, with enrichment in $APP^{L/S}$ mice and further enrichment with the addition of BD10-2. Turning to immune-related ontologies, upregulated genes in both APP and APP-BD10-2 effects were enriched in inflammatory, cytokines, and apoptotic terms. The APP-BD10-2 effect showed a mild decreased enrichment in inflammatory response and cytokine production, and a mild increased enrichment of complement and apoptotic processes, compared to the APP effect (Figure 7C). Last, regulation of neurogenesis, neuron death, and cell projection membrane show increased enrichment of up- and downregulated genes in the APP-BD10-2 effect compared to the APP effect. This carries forward into known LTP-associated spine turnover ontologies. There is a broad enrichment of neurogenesis and cell membrane projection, combined with increased complement pathway and apoptotic processes, suggestive of considerable synaptic/cellular turnover and endocytic activity (Figure 7C).

An overlap enrichment analysis was performed to determine whether DE genes (hereafter limited to *P*adj < 0.05) associated with the APP effect and the APP-BD10-2 effect were enriched for AD-relevant human-mouse co-expression modules.[58] This analysis revealed that neuronal human-mouse AD co-expression modules showed a mild enrichment in APP effect downregulated genes and a distinctly greater enrichment in APP-BD10-2 effect downregulated genes (Figure 7D, Figure S4B). This suggested that transcriptional changes observed in APP and APP-BD10-2 mice compared to WT-Veh mice occur in AD relevant genes. Microglial AD-relevant modules were strongly enriched in genes upregulated in both the APP effect and the APP-BD10-2 effect (Figure 7D). This finding demonstrates that BD10-2 and genotype both upregulate a number of broad scale immune processes regardless of whether the sample exhibited activity-dependent LTP. Upregulated genes in four additional oligodendroglial modules showed significant enrichment only in APP-BD10-2 effect upregulated genes, suggesting BD10-2 may be activating oligodendroglial processes (Figure 7D). Additionally, Milind et al.[105] iteratively re-clustered the Wan et al. AD co-expression modules to develop pathway-specific modules that we used for AD-related overlap enrichment (Figure S4C). Overlap enrichment for APP and APP-BD10-2 effect DE (*P*adj < 0.05) in these modules show similar patterns of immune response, synaptic signaling, as well as enrichment of upregulated oligodendroglial and cytoskeletal rearrangement modules. Together, we found that long-term dosing with BD10-2 imparts transcriptomic shifts in neuronal, microglial, and oligodendroglial, human-mouse AD co-expression modules that are otherwise smaller or absent when examining APP effect alone.

Co-expression modules in the DE gene sets were independently derived to examine their relationship to AD pathology using a weighted gene co-expression network analysis (Figure 8). This module-based assessment offers an additional approach for detection of shared expression changes associated with BD10-2 compared to assessment of the enrichment of individual DE genes. There were 23,407 genes expressed in hippocampal slices from the four groups: WT-Veh-TBS, APP-Veh-TBS, WT-BD10-2-TBS, and APP-BD10-2-TBS. Among these, 34 modules were detected and 28 of these had a minimum size of 50 genes (Figure 8A,B). Using the same effect comparisons that were used for the overlap enrichment analysis in Figure 7D (the APP effect and the APP-BD10-2 effect), there were five modules significantly associated with the APP effect and eight modules associated with the APP-BD10-2 effect (FDR < 0.05). Some of the strongest AD-related modules were significantly upregulated in both the APP effect and the APP-BD10-2 effect (red in upper panel of Figure 8B, Figure S1A). These modules showed more upregulation for the APP-BD10-2 effect versus the APP effect alone, echoing the above analyses. The three modules with the strongest upregulation (M2, M6, M18) had cell type–specific enrichment for microglia and astrocytes using an independent mouse cortex and hippocampus single-cell data set from Zhang et al.[57] (green in lower panel of Figure 8B). Module M6 showed a particularly strong effect and contained many of the top DE genes from our analysis of individual gene expression changes (Figure 7A), including *C1q* subunits, *Trem2*, *Gfap*, and *Tyrobp* (Figure 8C). Looking at pathway/ontology enrichment for highlighted modules in Figure 8D, we see M6 enriched for immune-associated function.

The five strongest downregulated co-expression modules (M15, M9, M4, M19, and M22) exhibited APP genotype–associated downregulation and even stronger APP-BD10-2–associated downregulation (blue in upper panel of Figure 8B), with two modules passing FDR significance (FDR < 0.05) for the APP-BD10-2 effect but not for the APP effect. These modules had significant cell type–specific enrichment for neurons (lower panel in Figure 8B), concurring with the enrichment in neuronal AD-related co-expression modules (Figure 7D). Modules

between the BD10-2 effect on the *x* axis and the APP effect on the *y* axis in genes that are nominally significant (*P* < 0.05) for both effects. C, Enrichment (g:SCS adjusted FDR) of selected ontologies/pathways relevant to LTP in downregulated (left) and upregulated (right) nominally significant (*P* < 0.05) DE genes for the three effect comparisons. D, Overlap enrichment (Fisher exact) of AD-related human-mouse co-expression modules from Wan et al.[58] compared to upregulated (top two rows)/downregulated (bottom two rows) DE genes (*P*adj < 0.05) in the APP effect and the APP-BD10-2 effect. Circles are sized and annotated with the Jaccard index of their overlap and are colored by the significance of the overlap enrichment (−log FDR; circles with an FDR < 0.05 have a bold edge). Modules are grouped based on "consensus clusters": yellow, astroglial-like modules; light blue, microglial-like modules; maroon, neuronal-associated modules; green, oligodendroglial-like modules. Modules are additionally annotated along the bottom by the associated brain region of the human AD cohort from which they were derived. AD, Alzheimer's disease; CBE, cerebellum; DE, differential gene expression; DLPFC, dorsolateral prefrontal cortex; FDR, false discovery rate; FP, frontal pole; IFG, inferior frontal gyrus; LTP, long-term potentiation; PHG, parahippocampal gyrus; STG, superior temporal gyrus; TBS, theta-burst stimulation; TCX, temporal cortex; Veh, vehicle; WT, wild type.

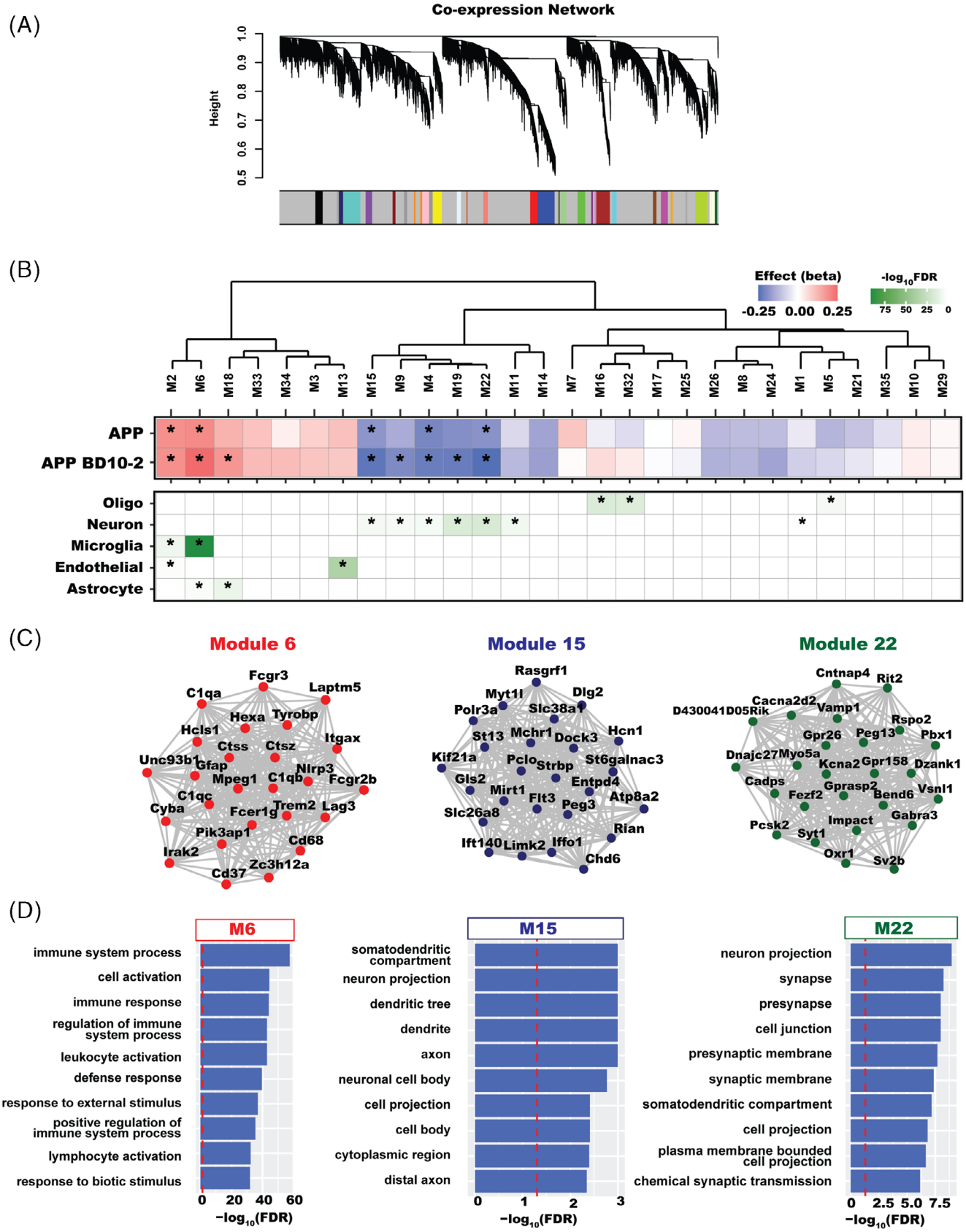

FIGURE 8 WGCNA of post-TBS hippocampal slices after 3 months in vivo BD10-2 treatment for 16-month-old $APP^{L/S}$ mice. A, Hierarchical cluster tree of 23,407 expressed genes in stimulated hippocampal slices from WT-Veh mice and $APP^{L/S}$ mice with or without BD10-2 treatment. The branches and color bands represent the 34 modules that were detected. B, Hierarchical clustering of gene co-expression modules by module eigengene in the APP effect (APP-Veh-TBS vs. WT-Veh-TBS) and the APP-BD10-2 effect (APP-BD10-2-TBS vs. WT-Veh-TBS). Only modules with a

M15 and M22 showed significant enrichment for dendrite, membrane projection, and synaptic genes (Figure 8C,D). Importantly, we also observed downregulation of synaptic genes and neuronal modules in the TBS effects from Figure 6, suggesting again that this is a hallmark of BD10-2–mediated LTP rescue in $APP^{L/S}$ mice.

4 | DISCUSSION

In the present study, we addressed the question of whether upregulation of TrkB/C receptor signaling, as achieved by administration of BD10-2, affects deficits in synaptic function present in $APP^{L/S}$ mice. In vitro studies determined that BD10-2 promotes hippocampal neuron survival to a similar extent as its parent compound LM22B-10. Hippocampal slice and in vivo studies demonstrated that activating TrkB/C with BD10-2 ameliorates LTP and memory deficits present in $APP^{L/S}$ mice in association with activating Akt and CaMKII signaling, restoring altered GluA1 phosphorylation and localization, and increasing number of excitatory synapses, all crucial to LTP. These effects occur in the absence of Aβ reduction, a profile consistent with the promotion of synaptic resilience. We also show that BD10-2 rescues activity-dependent, LTP-associated synaptic gene transcription and broadly activates transcription associated with microglial and immune pathways.

4.1 | APP and BD10-2 effects on signaling in late LTP

We first demonstrated that BD10-2 promotes cell survival acting through TrkB/TrkC receptors. It is well known that interaction of TrkB with its endogenous ligand BDNF modulates synaptic transmission and induces LTP.[71,106–109] Consistent with this effect of BDNF, we found that BD10-2 can prevent synaptic plasticity impairments and memory deficits that occur in aged $APP^{L/S}$ mice suggesting that BD10-2 mimics, in part, the biological effects of BDNF by activating TrkB/C. We found that major components of synaptic plasticity are restored in $APP^{L/S}$ mice by activating TrkB/C receptors in vivo, even though BD10-2 was not physically present at the time of slice recording. These findings suggest that BD10-2 might cause persistent structural and functional changes at synapses, contributing to functional recovery. Futures studies will assess the persistence of these changes.

Initiation of hippocampal LTP requires calcium-dependent activation of CaMKII at dendritic spines and surface insertion of synaptic AMPARs.[102,110–115] Late LTP involves gene expression, protein synthesis, and persistent biochemical alterations, leading to long-lasting synaptic changes.[71,116,117] LTP activates phosphorylation of many proteins such as CaMKII, GluA1-containing AMPARs, Akt, and ERK, which are crucial for maintaining synaptic plasticity through activity-induced protein synthesis regulation.[74,110,118–123] Aberrant regulation of these proteins has been reported in AD human brain and several AD mouse models.[124,125] BDNF-TrkB signaling activates many of these same pathways including the canonical three: PI3K/Akt, MAPK/ERK, and PLCγ/PKC pathways and is directly involved in the maintenance of L-LTP.[71] Notably, PLCγ/PKC pathway activation triggers Ca^{2+} influx, activating CaMKII, which is involved in LTP.[68–72] Signaling through PLCγ/PKC, MAPK/ERK, and PI3K/Akt pathways can all induce downstream activation of transcription factors such as cyclic-AMP responsive element binding protein (CREB) which promotes expression of genes required for LTP maintenance.[71,126–128] We examined the phosphorylation and levels of proteins involved in these three pathways (PI3K/Akt, MAPK/ERK, and PLCγ/PKC). Our data, consistent with Lee and Landreth,[129] indicates a significant decrease in the phosphorylation of GluA1 and its kinases CAMKII-α /-β as well as altered activity-dependent colocalization of GluA1 with the dendritic protein drebrin in $APP^{L/S}$ mice. Phosphorylation of GluA1 and CaMKII-β (but not CaMKII-α) was preserved at WT levels by chronic BD10-2 treatment. Drebrin is an actin-binding protein that promotes dendritic growth at excitatory post synapses.[130,131] AMPAR activity stabilizes drebrin in spines.[132] We demonstrated that modulation of TrkB/C receptors by BD10-2 treatment contributes to AMPAR-dependent stabilization of drebrin in spines as a novel activity-dependent mechanism for normalization of APP/Aβ-associated synaptic dysfunction. Remarkably, phosphorylation of CaMKII-β and Akt were decreased and restored by BD10-2 only in non-stimulated slices from $APP^{L/S}$ mice while GluA1 phosphorylation deficits in $APP^{L/S}$ mice was also restored by BD10-2 in stimulated slices indicating that rescue of GluA1 activation by BD10-2 is not activity dependent. In addition, chronic BD10-2 treatment mitigated the reduction in the number of excitatory synapses in $APP^{L/S}$ mice, by increasing colocalization of VGluT1 and PSD-95. This aligns with mechanisms consistent with strengthening synaptic function and/or boosting plasticity despite unchanged Aβ levels, potentially representing a form of resilience. Future experiments will explore the potential mechanisms underlying this proposed resilience. Perhaps rescue of baseline levels of CaMKII-β and Ak proteins is sufficient to restore downstream activity-dependent mechanisms such as synaptic recruitment of drebrin and activated AMPARs, as well as formation of new synapses to maintain LTP. Based on these findings, we propose a model, similar to what has been described previously for BDNF,[71] in which BD10-2 prevents APP/Aβ-induced deficits in L-LTP by promoting CaMKII and GluA1 phosphorylation/activation through activation of the TrkB/C-regulated PLCγ/PKC pathway, thereby rescuing

minimum size of 50 genes are shown. The plot below the dendrogram shows the module association strength with each effect. FDR < 0.05 for each module is denoted with an asterisk. A total of five modules were significantly associated with the APP effect. Three additional modules were significantly associated with the APP-BD10-2 effect. Module cell-type enrichments (*FDR < 0.05) are shown in the panel below for major CNS cell types. C, Examples of specific modules dysregulated across APP and APP-BD10-2 effects, with the top 25 hub genes shown. D, Top 10 GO enrichments for genes in modules 6, 15, and 22, red dashed line indicates FDR < 0.05 significance. CNS, central nervous system; FDR, false discover rate; GO, Gene Ontology; TBS, theta-burst stimulation; Veh, vehicle; WGCNA, weighted gene co-expression network analysis; WT, wild type.

activity dependent AMPAR/drebrin and VGlut1/PSD-95 colocalization in dendritic spines. Future experiments examining earlier time points post-TBS could provide crucial insights into how rapidly BD10-2 impacts the transient phosphorylation events involved in plasticity.

4.2 | Effects of APP and BD10-2 on activity-dependent late LTP associated transcription

We next asked whether $APP^{L/S}$ expression (described here as the APP effect) and/or BD10-2 influenced activity-dependent LTP associated gene expression which is required to support protein synthesis alterations needed for long-lasting synaptic changes occurring in L-LTP. RNA-seq on 120 minute post-TBS hippocampal slices revealed LTP-dependent downregulation of genes involved in synaptic signaling and potentiation. We found a clear transcriptomic signature of LTP that is not found in slices that did not undergo LTP (TBS−): occurring in WT-Veh mice, altered in APP-Veh mice, and restored in APP-BD10-2 mice. Overlap enrichment analysis revealed that these transcriptional changes overlap with neuronal modules previously determined to have relevance to AD. Direct comparison of TBS+ slices for the APP effect and the APP-BD10-2 effect also showed that this signature was present only with BD10-2, further implicating BD10-2 in LTP rescue in an AD context. Together with direct observation of LTP on these same hippocampal slices, we see a measurable and lasting transcriptomic impact during the rescue of LTP by BD10-2.

4.3 | Transcriptional effects of APP and BD10-2 on microglial genes in the context of LTP

We observed strong upregulation of broad sets of immune-relevant genes and pathways with TBS regardless of whether the samples had measurable LTP. Compared to WT, these pathways exhibited stronger upregulation in $APP^{L/S}$ mice with and without BD10-2 suggesting this immune upregulation is not activity dependent but may be correlated with amyloid pathology. Overlap enrichment analysis and network module analysis of the APP effect in stimulated samples reiterated this broad upregulation of AD-relevant genes but only mildly increases with BD10-2. However, microglia-associated pathways—including the complement pathway—were more enriched in response to BD10-2 and stimulation.

Notable genes that were upregulated in both the APP effect and further upregulated in the APP-BD10-2 effect include *Clec7a* and *Cst7*, two markers of disease-associated microglia.[133–135] Our data also identify a gene transcription module (M6red), which is enriched for a large set of complement genes that have previously been linked to microglial response to Aβ: *Trem2*, *Tyrobp*, *Cd68*, *C1qa*, *C1qb*, *C1qc*, and *C3*. Microglia are the dominant immune cell type in the brain[136] and they play a major role in Aβ clearance.[129] Moving beyond amyloid, one of the top DE genes in the BD10-2 effect itself was *C3*, still significantly upregulated over 24 hours after BD10-2 clearance from the brain, suggesting a lasting engagement of this specific complement mechanism. *C3* has been shown to label synapses targeted for synaptic pruning, involving the complement system directly in synapse elimination as a result of LTP-promoted spine turnover.[137,138] Alterations in the complement system have been observed in AD patients[139] and AD mice,[98] and excessive synaptic elimination in AD suggests the complement system balances microglial response between protective and detrimental.[140–143] Upregulation of these complement genes was correlated with an enrichment of neurogenesis, apoptosis, and neurotrophin pathways impacting synaptic plasticity/turnover, but further studies are needed to understand the mechanisms by which LTP may drive this balance.

4.4 | Limitations and conclusions

Activating the TrkB/C receptor is a promising strategy for translational drug development considering it rescues synaptic function and cognition in mice with late-stage pathology. This study presents a novel small molecule ligand, BD10-2, whose parent compound (LM22B-10) activates TrkB/TrkC receptors. To our knowledge, other compounds activating TrkB and C have not been developed, and future studies will further explore this approach. A potential limitation in the application of BD10-2 includes off-target effects, although a competition binding assay screening 44 common receptors detected no off-target binding.[25] Adverse events related to TrkB/C signaling including weight loss or behavioral change are possible, although changes in these outcomes were not observed here.

We found that activating TrkB/C receptors with BD10-2 rescues LTP and cognition, modulates LTP-associated pathways downstream of TrkB signaling, and alters activity-dependent gene expression. To assess the large volume of data generated in our RNA-seq studies of transcriptional changes that occur in L-LTP, we focused on analyzing broad changes in related genes using various computational methods; however, it is possible we are missing more granular changes that occur in specific genes or pathways. Our data generate new questions surrounding activity-dependent transcription of synaptic and immune programs during LTP that will need to be explored in future studies, especially in the context of AD pathophysiology and therapeutic target development.

AUTHOR CONTRIBUTIONS

Amira Latif-Hernandez and Tao Yang designed and performed experiments and analyzed the data. Amira Latif-Hernandez designed, peformed, analyzed, graphed and interpreted electrophysiology experiments, collected all the tissue post-stimulation and coordinated all the collaborations. Tao Yang executed western blotting experiments. Paras Minhas performed behavioral experiments and analyzed the data. Robert R. Butler III, Patricia Moran-Losada, and Tony Wyss-Coray analyzed the RNA-seq data. Halle White contributed to analysis of one data set of immunostaining data. Kevin C. Tran and Harry Liu administered the compound to the four cohorts of animals. Amira Latif-Hernandez, Tao Yang, Robert R. Butler III, Vanessa Langness, and Danielle A. Simmons wrote the manuscript. Amira Latif-Hernandez and Frank M. Longo conceived and supervised the project, designed the study, interpreted the data, and finalized the manuscript.

ACKNOWLEDGMENTS

We would like to thank the Stanford Functional Genomics Facility for performing the RNA-seq experiments. Some of the computing for this project was performed on the Stanford SCG cluster. We would like to thank the Stanford Research Computing Center for providing computational resources and support. Wan et al. network modules were based on data obtained from the AD Knowledge Portal. Data generation was supported by the following NIH grants: P30AG10161, P30AG72975, R01AG15819, R01AG17917, R01AG036836, U01AG46152, U01AG61356, U01AG046139, P50 AG016574, R01 AG032990, U01AG046139, R01AG018023, U01AG006576, U01AG006786, R01AG025711, R01AG017216, R01AG003949, R01NS080820, U24NS072026, P30AG19610, U01AG046170, RF1AG057440, and U24AG061340, and the Cure PSP, Mayo and Michael J Fox foundations, Arizona Department of Health Services, and the Arizona Biomedical Research Commission. We thank the participants of the Religious Order Study and Memory and Aging projects for the generous donation, the Sun Health Research Institute Brain and Body Donation Program, the Mayo Clinic Brain Bank, and the Mount Sinai/JJ Peters VA Medical Center NIH Brain and Tissue Repository. Data and analysis contributing investigators include Nilüfer Ertekin-Taner, Steven Younkin (Mayo Clinic, Jacksonville, FL), Todd Golde (University of Florida), Nathan Price (Institute for Systems Biology), David Bennett, Christopher Gaiteri (Rush University), Philip De Jager (Columbia University), Bin Zhang, Eric Schadt, Michelle Ehrlich, Vahram Haroutunian, Sam Gandy (Icahn School of Medicine at Mount Sinai), Koichi Iijima (National Center for Geriatrics and Gerontology, Japan), Scott Noggle (New York Stem Cell Foundation), Lara Mangravite (Sage Bionetworks). We express our special gratitude to Tariq Ahmed for his profound intellectual contributions and innovative scientific insights, which were instrumental in deciphering the synaptic mechanisms proposed in this paper. Additionally, we appreciate his invaluable supervision and guidance during the execution of electrophysiology experiments, which greatly advanced our research. This work was supported by funds from the Scully Initiative, Taube Family Foundation, Jean Perkins Foundation, Applebaum Foundation, the Horngren Family, as well as funding from 5T32GM007365-45 and Stanford Alzheimer's Disease Research Center Grant P30 AG066515 | SPO 147289.

CONFLICT OF INTEREST STATEMENT

F.M.L. is listed as an inventor on patents covering LM22B-10 and PTX-BD10-2. F.M.L. is a principal of, and has financial interest in, PharmatrophiX, a company with ownership and/or licensing rights to these patents. A.L.H., T.Y., R.R.B., P.M.L., P.M., H.W., K.C.T., H.L., D.A.S., V.F.L., and T.W.C. declare no conflicts of interest. Author disclosures are available in the supporting information.

CONSENT STATEMENT

Consent from human subjects was not necessary.

REFERENCES

1. Koffie RM, Hyman BT, Spires-Jones TL. Alzheimer's disease: synapses gone cold. *Mol Neurodegener*. 2011;6:63.
2. Selkoe DJ. Alzheimer's disease is a synaptic failure. *Science*. 2002;298:789-791.
3. Medawar E, Benway TA, Liu W, et al. Effects of rising amyloidbeta levels on hippocampal synaptic transmission, microglial response and cognition in APP(Swe)/PSEN1(M146V) transgenic mice. *EBioMedicine*. 2019;39:422-435.
4. Puzzo D, Piacentini R, Fa M, et al. LTP and memory impairment caused by extracellular Abeta and Tau oligomers is APP-dependent. *eLife*. 2017;6:e26991.
5. Cummings DM, Liu W, Portelius E, et al. First effects of rising amyloid-beta in transgenic mouse brain: synaptic transmission and gene expression. *Brain*. 2015;138:1992-2004.
6. Crouzin N, Baranger K, Cavalier M, et al. Area-specific alterations of synaptic plasticity in the 5XFAD mouse model of Alzheimer's disease: dissociation between somatosensory cortex and hippocampus. *PLoS One*. 2013;8:e74667.
7. Latif-Hernandez A, Sabanov V, Ahmed T, et al. The two faces of synaptic failure in AppNL-G-F knock-in mice. *Alzheimers Res Ther*. 2020;12(1):100.
8. Cullen WK, Suh YH, Anwyl R, Rowan MJ. Block of LTP in rat hippocampus in vivo by beta-amyloid precursor protein fragments. *Neuroreport*. 1997;8:3213-3217.
9. Nalbantoglu J, Tirado-Santiago G, Lahsaïni A, et al. Impaired learning and LTP in mice expressing the carboxy terminus of the Alzheimer amyloid precursor protein. *Nature*. 1997;387:500-505.
10. Crimins JL, Pooler A, Polydoro M, Luebke JI, Spires-Jones TL. The intersection of amyloid beta and tau in glutamatergic synaptic dysfunction and collapse in Alzheimer's disease. *Ageing Res Rev*. 2013;12:757-763.
11. Lu B, Pang PT, Woo NH. The yin and yang of neurotrophin action. *Nat Rev Neurosci*. 2005;6:603-614.
12. Huang SH, Wang J, Sui WH, et al. BDNF-dependent recycling facilitates TrkB translocation to postsynaptic density during LTP via a Rab11-dependent pathway. *J Neurosci*. 2013;33:9214-9230.
13. Rose CR, Blum R, Kafitz KW, Kovalchuk Y, Konnerth A. From modulator to mediator: rapid effects of BDNF on ion channels. *Bioessays*. 2004;26:1185-1194.
14. Hernandez-Echeagaray E. Neurotrophin-3 modulates synaptic transmission. *Vitam Horm*. 2020;114:71-89.
15. Je HS, Ji Y, Wang Y, Yang F, Wu W, Lu B. Presynaptic protein synthesis required for NT-3-induced long-term synaptic modulation. *Mol Brain*. 2011;4:1. doi:10.1186/1756-6606-4-1
16. Wang Z-H, Xiang J, Liu X, et al. Deficiency in BDNF/TrkB neurotrophic activity stimulates δ-secretase by upregulating C/EBPβ in Alzheimer's disease. *Cell Rep*. 2019;28:655-669.e5.
17. Numakawa T, Odaka H. The role of neurotrophin signaling in age-related cognitive decline and cognitive diseases. *Int J Mol Sci*. 2022;23:7726.
18. Amidfar M, de Oliveira J, Kucharska E, Budni J, Kim YK. The role of CREB and BDNF in neurobiology and treatment of Alzheimer's disease. *Life Sci*. 2020;257:118020.
19. Simmons DA, Yang T, Massa SM, Longo FM. Neuroprotective strategies for Alzheimer's disease prevention and therapy. *Developing Therapeutics for Alzheimer's Disease*. Elsevier; 2016:437-458. https://shop.elsevier.com/books/developing-therapeutics-for-alzheimers-disease/wolfe/978-0-12-802173-6
20. Longo FM, Massa SM. Small-molecule modulation of neurotrophin receptors: a strategy for the treatment of neurological disease. *Nat Rev Drug Discov*. 2013;12:507-525.

21. Zagrebelsky M, Korte M. Are TrkB receptor agonists the right tool to fulfill the promises for a therapeutic value of the brain-derived neurotrophic factor? *Neural Regen Res*. 2024;19:29-34.
22. Antonijevic M, Charou D, Ramos I, et al. Design, synthesis and biological characterization of novel activators of the TrkB neurotrophin receptor. *Eur J Med Chem*. 2023;248:115111.
23. Lu B, Nagappan G, Guan X, Nathan PJ, Wren P. BDNF-based synaptic repair as a disease-modifying strategy for neurodegenerative diseases. *Nat Rev Neurosci*. 2013;14:401-416.
24. Yang T, Massa SM, Tran KC, et al. A small molecule TrkB/TrkC neurotrophin receptor co-activator with distinctive effects on neuronal survival and process outgrowth. *Neuropharmacology*. 2016;110:343-361.
25. Gonzalez S, McHugh TLM, Yang T, et al. Small molecule modulation of TrkB and TrkC neurotrophin receptors prevents cholinergic neuron atrophy in an Alzheimer's disease mouse model at an advanced pathological stage. *Neurobiol Dis*. 2022;162:105563.
26. Simmons DA, Belichenko NP, Longo FM. Pharmacological co-activation of TrkB and TrkC receptor signaling ameliorates striatal neuropathology and motor deficits in mouse models of Huntington's disease. *J Huntingtons Dis*. 2023;12:215-239.
27. Rockenstein E, Mallory M, Mante M, Sisk A, Masliaha E. Early formation of mature amyloid-beta protein deposits in a mutant APP transgenic model depends on levels of Abeta(1-42). *J Neurosci Res*. 2001;66:573-582.
28. Nguyen TV, Shen L, Vander Griend L, et al. Small molecule p75NTR ligands reduce pathological phosphorylation and misfolding of tau, inflammatory changes, cholinergic degeneration, and cognitive deficits in AbetaPP(L/S) transgenic mice. *J Alzheimers Dis*. 2014;42:459-483.
29. Yang T, Massa SM, Longo FM. LAR protein tyrosine phosphatase receptor associates with TrkB and modulates neurotrophic signaling pathways. *J Neurobiol*. 2006;66:1420-1436.
30. Yang T, Knowles JK, Lu Q, et al. Small molecule, non-peptide p75NTR ligands inhibit Aβ-induced neurodegeneration and synaptic impairment. *PLoS One*. 2008;3:e3604.
31. Walter J, Keiner S, Witte OW, Redecker C. Age-related effects on hippocampal precursor cell subpopulations and neurogenesis. *Neurobiol Aging*. 2011;32:1906-1914.
32. Massa SM. Small, Nonpeptide p75NTR Ligands Induce Survival Signaling and Inhibit proNGF-Induced Death. *J Neurosci*. 2006;26:5288-5300.
33. Havas D, Hutter-Paier B, Ubhi K, et al. A longitudinal study of behavioral deficits in an AbetaPP transgenic mouse model of Alzheimer's disease. *J Alzheimers Dis*. 2011;25:231-243.
34. Knowles JK, Simmons DA, Nguyen TV, et al. Small molecule p75NTR ligand prevents cognitive deficits and neurite degeneration in an Alzheimer's mouse model. *Neurobiol Aging*. 2013;34:2052-2063.
35. Simmons DA, Knowles JK, Belichenko NP, et al. A Small molecule p75NTR ligand, LM11A-31, reverses cholinergic neurite dystrophy in Alzheimer's disease mouse models with mid- to late-stage disease progression. *PLoS One*. 2014;9:e102136.
36. Dere E, Huston JP, De Souza Silva MA. Integrated memory for objects, places, and temporal order: evidence for episodic-like memory in mice. *Neurobiol Learn Mem*. 2005;84:214-221.
37. Attar A, Liu T, Chan W-TC, et al. A shortened Barnes maze protocol reveals memory deficits at 4-months of age in the triple-transgenic mouse model of Alzheimer's disease. *PLoS One*. 2013;8:e80355.
38. Minhas PS, Latif-Hernandez A, McReynolds MR, et al. Restoring metabolism of myeloid cells reverses cognitive decline in ageing. *Nature*. 2021;590:122-128.
39. Iweka CA, Seigneur E, Hernandez AL, et al. Myeloid deficiency of the intrinsic clock protein BMAL1 accelerates cognitive aging by disrupting microglial synaptic pruning. *J Neuroinflammation*. 2023;20:48.
40. ENCODE. Bulk RNA-seq data standards and processing pipeline. 2017.
41. Hitz BC, Jin-Wook L, Jolanki O, et al. The ENCODE uniform analysis pipelines. *Biorxiv*. 2023. doi:10.1101/2023.04.04.535623
42. Martin M. Cutadapt removes adapter sequences from high-throughput sequencing reads. *EMBnetjournal*. 2011;17(1):10-12.
43. Dobin A, Davis CA, Schlesinger F, et al. STAR: ultrafast universal RNA-seq aligner. *Bioinformatics*. 2013;29:15-21.
44. Li B, Dewey CN. RSEM: accurate transcript quantification from RNA-Seq data with or without a reference genome. *BMC Bioinf*. 2011;12:323.
45. Liao Y, Smyth GK, Shi W. featureCounts: an efficient general purpose program for assigning sequence reads to genomic features. *Bioinformatics*. 2014;30:923-930.
46. Institute B. Picard Toolkit. Broad Institute, Github repository; 2019. https://github.com/broadinstitute/picard/tree/3.1.1
47. Danecek P, Bonfield JK, Liddle J, et al. Twelve years of SAMtools and BCFtools. *Gigascience*. 2021;10(2):giab008.
48. Team RC. *R: A Language and Environment for Statistical Computing*. R Foundation for Statistical Computing; 2018.
49. Witten DM. Classification and clustering of sequencing data using a Poisson model. *Ann Appl Stat*. 2011;5:2493-2518.
50. Oldham MC, Langfelder P, Horvath S. Network methods for describing sample relationships in genomic datasets: application to Huntington's disease. *BMC Syst Biol*. 2012;6:63.
51. Love MI, Huber W, Anders S. Moderated estimation of fold change and dispersion for RNA-seq data with DESeq2. *Genome Biol*. 2014;15:550.
52. Durinck S, Spellman PT, Birney E, Huber W. Mapping identifiers for the integration of genomic datasets with the R/Bioconductor package biomaRt. *Nat Protoc*. 2009;4:1184-1191.
53. Raudvere U, Kolberg L, Kuzmin I, et al. g:Profiler: a web server for functional enrichment analysis and conversions of gene lists (2019 update). *Nucleic Acids Res*. 2019;47:W191-W198.
54. Langfelder P, Horvath S. WGCNA: an R package for weighted correlation network analysis. *BMC Bioinf*. 2008;9:559.
55. Goldmann T, Wieghofer P, Jordão MJC, et al. Origin, fate and dynamics of macrophages at central nervous system interfaces. *Nat Immunol*. 2016;17:797-805.
56. Zeisel A, Munoz-Manchado AB, Codeluppi S, et al. Brain structure. Cell types in the mouse cortex and hippocampus revealed by single-cell RNA-seq. *Science*. 2015;347:1138-1142.
57. Zhang Y, Sloan SA, Clarke LE, et al. Purification and characterization of progenitor and mature human astrocytes reveals transcriptional and functional differences with mouse. *Neuron*. 2016;89:37-53.
58. Wan YW, Al-Ouran R, Mangleburg CG, et al. Meta-analysis of the Alzheimer's disease human brain transcriptome and functional dissection in mouse models. *Cell Rep*. 2020;32:107908.
59. Shen L, Sinai ISoMaM. GeneOverlap: test and visualize gene overlaps. R package version 1.26.0. 2020. https://new.bioconductor.org/packages/release/bioc/html/GeneOverlap.html
60. Lu B. BDNF and activity-dependent synaptic modulation. *Learn Mem*. 2003;10(2):86-98.
61. Aloyz R, Fawcett JP, Kaplan DR, Murphy RA, Miller FD. Activity-dependent activation of TrkB neurotrophin receptors in the adult CNS. *Learn Mem*. 1999;6:216-231.
62. Denayer E, Ahmed T, Brems H, et al. Spred1 is required for synaptic plasticity and hippocampus-dependent learning. *J Neurosci*. 2008;28:14443-14449.
63. Larson J, Lynch G. Theta pattern stimulation and the induction of LTP: the sequence in which synapses are stimulated determines the degree to which they potentiate. *Brain Res*. 1989;489:49-58.
64. Buzsáki G, Moser EI. Memory, navigation and theta rhythm in the hippocampal-entorhinal system. *Nat Neurosci*. 2013;16:130-138.
65. Bourne JN, Harris KM. Coordination of size and number of excitatory and inhibitory synapses results in a balanced structural plasticity along mature hippocampal CA1 dendrites during LTP. *Hippocampus*. 2011;21:354-373.

66. Larson J, Xiao P, Lynch G. Reversal of LTP by theta frequency stimulation. *Brain Res*. 1993;600:97-102.
67. Malinow R, Malenka RC. AMPA receptor trafficking and synaptic plasticity. *Annu Rev Neurosci*. 2002;25:103-126.
68. Gomes AR, Correia SS, Carvalho AL, Duarte CB. Regulation of AMPA receptor activity, synaptic targeting and recycling: role in synaptic plasticity. *Neurochem Res*. 2003;28:1459-1473.
69. Zhang H, Zhang C, Vincent J, et al. Modulation of AMPA receptor surface diffusion restores hippocampal plasticity and memory in Huntington's disease models. *Nat Commun*. 2018;9:4272.
70. Tian M, Zeng Y, Hu Y, et al. 7, 8-Dihydroxyflavone induces synapse expression of AMPA GluA1 and ameliorates cognitive and spine abnormalities in a mouse model of fragile X syndrome. *Neuropharmacology*. 2015;89:43-53.
71. Minichiello L. TrkB signalling pathways in LTP and learning. *Nat Rev Neurosci*. 2009;10:850-860.
72. Caldeira MV, Melo CV, Pereira DB, et al. Brain-derived neurotrophic factor regulates the expression and synaptic delivery of alpha-amino-3-hydroxy-5-methyl-4-isoxazole propionic acid receptor subunits in hippocampal neurons. *J Biol Chem*. 2007;282:12619-12628.
73. Jackson J, Jambrina E, Li J, et al. Targeting the synapse in Alzheimer's disease. *Front Neurosci*. 2019;13:735.
74. Kelleher RJ, Govindarajan A, Tonegawa S. Translational regulatory mechanisms in persistent forms of synaptic plasticity. *Neuron*. 2004;44:59-73.
75. Li M, Dai FR, Du XP, Yang QD, Zhang X, Chen Y. Infusion of BDNF into the nucleus accumbens of aged rats improves cognition and structural synaptic plasticity through PI3K-ILK-Akt signaling. *Behav Brain Res*. 2012;231:146-153.
76. Yin Y, Gao D, Wang Y, et al. Tau accumulation induces synaptic impairment and memory deficit by calcineurin-mediated inactivation of nuclear CaMKIV/CREB signaling. *Proc Natl Acad Sci USA*. 2016;113:E3773-E3781.
77. Muraleva NA, Kolosova NG, Stefanova NA. MEK1/2-ERK pathway alterations as a therapeutic target in sporadic Alzheimer's disease: a study in senescence-accelerated OXYS rats. *Antioxidants*. 2021;10(7):1058.
78. Du Y, Du Y, Zhang Y, et al. MKP-1 reduces Aβ generation and alleviates cognitive impairments in Alzheimer's disease models. *Signal Transduct Target Ther*. 2019;4:58.
79. Zhu X, Lee HG, Raina AK, Perry G, Smith MA. The role of mitogen-activated protein kinase pathways in Alzheimer's disease. *Neurosignals*. 2002;11:270-281.
80. Fortin DA, Srivastava T, Dwarakanath D, et al. Brain-derived neurotrophic factor activation of CaM-kinase kinase via transient receptor potential canonical channels induces the translation and synaptic incorporation of GluA1-containing calcium-permeable AMPA receptors. *J Neurosci*. 2012;32:8127-8137.
81. Rodrigues NC, Silva-Cruz A, Caulino-Rocha A, Bento-Oliveira A, Alexandre Ribeiro J, Cunha-Reis D. Hippocampal CA1 theta burst-induced LTP from weaning to adulthood: Cellular and molecular mechanisms in young male rats revisited. *Eur J Neurosci*. 2021;54:5272-5292.
82. Zhang N, Shen Y, Zhu W, et al. Spatial transcriptomics shows moxibustion promotes hippocampus astrocyte and neuron interaction. *Life Sci*. 2022;310:121052.
83. Algamal M, Russ AN, Miller MR, et al. Reduced excitatory neuron activity and interneuron-type-specific deficits in a mouse model of Alzheimer's disease. *Commun Biol*. 2022;5:1323.
84. Meftah S, Gan J. Alzheimer's disease as a synaptopathy: Evidence for dysfunction of synapses during disease progression. *Front Synaptic Neurosci*. 2023;15:1129036.
85. Cai W, Li L, Sang S, Pan X, Zhong C. Physiological Roles of beta-amyloid in Regulating Synaptic Function: Implications for AD Pathophysiology. *Neurosci Bull*. 2023;39:1289-1308.
86. Frey U, Krug M, Reymann KG, Matthies H. Anisomycin, an inhibitor of protein synthesis, blocks late phases of LTP phenomena in the hippocampal CA1 region in vitro. *Brain Res*. 1988;452:57-65.
87. Huang YY, Kandel ER. Recruitment of long-lasting and protein kinase A-dependent long-term potentiation in the CA1 region of hippocampus requires repeated tetanization. *Learn Mem*. 1994;1:74-82.
88. Malenka RC, Nicoll RA. NMDA-receptor-dependent synaptic plasticity: multiple forms and mechanisms. *Trends Neurosci*. 1993;16:521-527.
89. Scharf MT, Woo NH, Lattal KM, Young JZ, Nguyen PV, Abel T. Protein synthesis is required for the enhancement of long-term potentiation and long-term memory by spaced training. *J Neurophysiol*. 2002;87:2770-2777.
90. Vickers CA, Wyllie DJA. Late-phase, protein synthesis-dependent long-term potentiation in hippocampal CA1 pyramidal neurones with destabilized microtubule networks. *Br J Pharmacol*. 2007;151:1071-1077.
91. Lu Y, Christian K, Lu B. BDNF: a key regulator for protein synthesis-dependent LTP and long-term memory? *Neurobiol Learn Mem*. 2008;89:312-323.
92. Bliss TVP, Collingridge GL, Morris RGM, Reymann KG. Long-term potentiation in the hippocampus: discovery, mechanisms and function. *Neuroforum*. 2018;24:A103-A120.
93. Fonkeu Y, Kraynyukova N, Hafner A-S, et al. How mRNA localization and protein synthesis sites influence dendritic protein distribution and dynamics. *Neuron*. 2019;103:1109-1122.e7.
94. Cao G, Harris KM. Developmental regulation of the late phase of long-term potentiation (L-LTP) and metaplasticity in hippocampal area CA1 of the rat. *J Neurophysiol*. 2012;107:902-912.
95. De Jager PL, Ma Y, McCabe C, et al. A multi-omic atlas of the human frontal cortex for aging and Alzheimer's disease research. *Sci Data*. 2018;5:180142.
96. Wang M, Beckmann ND, Roussos P, et al. The Mount Sinai cohort of large-scale genomic, transcriptomic and proteomic data in Alzheimer's disease. *Sci Data*. 2018;5:180185.
97. Allen M, Carrasquillo MM, Funk C, et al. Human whole genome genotype and transcriptome data for Alzheimer's and other neurodegenerative diseases. *Sci Data*. 2016;3:160089.
98. Matarin M, Salih DA, Yasvoina M, et al. A genome-wide gene-expression analysis and database in transgenic mice during development of amyloid or tau pathology. *Cell Rep*. 2015;10:633-644.
99. Kakinuma N, Zhu Y, Wang Y, Roy BC, Kiyama R. Kank proteins: structure, functions and diseases. *Cell Mol Life Sci*. 2009;66:2651-2659.
100. Zhang S, Cooper-Knock J, Weimer AK, et al. Genome-wide identification of the genetic basis of amyotrophic lateral sclerosis. *Neuron*. 2022;110:992-1008.e11.
101. Tang M, Li J, He L, et al. Transcriptomic profiling of neural stem cell differentiation on graphene substrates. *Colloids Surf B Biointerfaces*. 2019;182:110324.
102. McLeod F, Bossio A, Marzo A, et al. Wnt Signaling Mediates LTP-Dependent Spine Plasticity and AMPAR Localization through Frizzled-7 Receptors. *Cell Rep*. 2018;23:1060-1071.
103. Thomas GM, Huganir RL. MAPK cascade signalling and synaptic plasticity. *Nat Rev Neurosci*. 2004;5:173-183.
104. Sanchez-Alegria K, Flores-Leon M, Avila-Munoz E, Rodriguez-Corona N, Arias C. PI3K signaling in neurons: a central node for the control of multiple functions. *Int J Mol Sci*. 2018;19(12):3725.
105. Milind N, Preuss C, Haber A, et al. Transcriptomic stratification of late-onset Alzheimer's cases reveals novel genetic modifiers of disease pathology. *PLoS Genet*. 2020;16:e1008775.
106. Colucci-D'Amato L, Speranza L, Volpicelli F. Neurotrophic factor BDNF, physiological functions and therapeutic potential in depression, neurodegeneration and brain cancer. *Int J Mol Sci*. 2020;21:7777.

107. Levine ES, Dreyfus CF, Black IB, Plummer MR. Brain-derived neurotrophic factor rapidly enhances synaptic transmission in hippocampal neurons via postsynaptic tyrosine kinase receptors. *Proc Natl Acad Sci*. 1995;92:8074-8077.
108. Akaneya Y, Tsumoto T, Kinoshita S, Hatanaka H. Brain-derived neurotrophic factor enhances long-term potentiation in rat visual cortex. *J Neurosci*. 1997;17:6707-6716.
109. Choi SH, Bylykbashi E, Chatila ZK, et al. Combined adult neurogenesis and BDNF mimic exercise effects on cognition in an Alzheimer's mouse model. *Science*. 2018;361(6406):eaan8821.
110. Huganir RL, Nicoll RA. AMPARs and synaptic plasticity: the last 25 years. *Neuron*. 2013;80:704-717.
111. Opazo P, Labrecque S, Tigaret CM, et al. CaMKII triggers the diffusional trapping of surface AMPARs through phosphorylation of Stargazin. *Neuron*. 2010;67:239-252.
112. Barria A, Muller D, Derkach V, Griffith LC, Soderling TR. Regulatory phosphorylation of AMPA-type glutamate receptors by CaM-KII during long-term potentiation. *Science*. 1997;276:2042-2045.
113. Wu D, Bacaj T, Morishita W, et al. Postsynaptic synaptotagmins mediate AMPA receptor exocytosis during LTP. *Nature*. 2017;544:316-321.
114. Harris KM. Calcium from internal stores modifies dendritic spine shape. *Proc Natl Acad Sci USA*. 1999;96:12213-12215.
115. Paulin JJ, Haslehurst P, Fellows AD, et al. Large and small dendritic spines serve different interacting functions in hippocampal synaptic plasticity and homeostasis. *Neural Plast*. 2016;2016:6170509.
116. Bramham CR, Worley PF, Moore MJ, Guzowski JF. The immediate early genearc/arg3.1: regulation, mechanisms, and function. *J Neurosci*. 2008;28:11760-11767.
117. Larson J, Munkácsy E. Theta-burst LTP. *Brain Res*. 2015;1621:38-50.
118. Giovannini MG, Blitzer RD, Wong T, et al. Mitogen-activated protein kinase regulates early phosphorylation and delayed expression of Ca2+/calmodulin-dependent protein kinase II in long-term potentiation. *J Neurosci*. 2001;21:7053-7062.
119. Sweatt JD. Mitogen-activated protein kinases in synaptic plasticity and memory. *Curr Opin Neurobiol*. 2004;14:311-317.
120. Kelleher RJ, Govindarajan A, Jung H-Y, Kang H, Tonegawa S. Translational control by MAPK signaling in long-term synaptic plasticity and memory. *Cell*. 2004;116:467-479.
121. Henley JM, Wilkinson KA. AMPA receptor trafficking and the mechanisms underlying synaptic plasticity and cognitive aging. *Dialogues Clin Neurosci*. 2013;15:11-27.
122. Moriguchi S, Tagashira H, Sasaki Y, et al. CaMKII activity is essential for improvement of memory-related behaviors by chronic rivastigmine treatment. *J Neurochem*. 2014;128:927-937.
123. Levenga J, Wong H, Milstead RA, Keller BN, Laplante LE, Hoeffer CA. AKT isoforms have distinct hippocampal expression and roles in synaptic plasticity. *eLife*. 2017;6:e30640.
124. Griffin RJ, Moloney A, Kelliher M, et al. Activation of Akt/PKB, increased phosphorylation of Akt substrates and loss and altered distribution of Akt and PTEN are features of Alzheimer's disease pathology. *J Neurochem*. 2005;93:105-117.
125. Jurado S. AMPA receptor trafficking in natural and pathological aging. *Front Mol Neurosci*. 2017;10:446.
126. Du K, Montminy M. CREB is a regulatory target for the protein kinase Akt/PKB. *J Biol Chem*. 1998;273:32377-32379.
127. Rosa E, Fahnestock M. CREB expression mediates amyloid beta-induced basal BDNF downregulation. *Neurobiol Aging*. 2015;36:2406-2413.
128. Ying SW, Futter M, Rosenblum K, et al. Brain-derived neurotrophic factor induces long-term potentiation in intact adult hippocampus: requirement for ERK activation coupled to CREB and upregulation of Arc synthesis. *J Neurosci*. 2002;22:1532-1540.
129. Lee CYD, Landreth GE. The role of microglia in amyloid clearance from the AD brain. *J Neural Transm*. 2010;117:949-960.
130. Takahashi H, Sekino Y, Tanaka S, Mizui T, Kishi S, Shirao T. Drebrin-dependent actin clustering in dendritic filopodia governs synaptic targeting of postsynaptic density-95 and dendritic spine morphogenesis. *J Neurosci*. 2003;23:6586-6595.
131. Takahashi H, Naito Y. *Drebrin and Spine Formation*. Japan: Springer; 2017:157-181.
132. Takahashi H, Yamazaki H, Hanamura K, Sekino Y, Shirao T. Activity of the AMPA receptor regulates drebrin stabilization in dendritic spine morphogenesis. *J Cell Sci*. 2009;122:1211-1219.
133. Clayton K, Delpech JC, Herron S, et al. Plaque associated microglia hyper-secrete extracellular vesicles and accelerate tau propagation in a humanized APP mouse model. *Mol Neurodegener*. 2021;16(1):18.
134. Grubman A, Choo XY, Chew G, et al. Transcriptional signature in microglia associated with Aβ plaque phagocytosis. *Nat Commun*. 2021;12(1):3015.
135. Deczkowska A, Keren-Shaul H, Weiner A, Colonna M, Schwartz M, Amit I. Disease-associated microglia: a universal immune sensor of neurodegeneration. *Cell*. 2018;173:1073-1081.
136. Morimoto K, Nakajima K. Role of the immune system in the development of the central nervous system. *Front Neurosci*. 2019;13:916.
137. Cardozo PL, de Lima IBQ, Maciel EMA, Silva NC, Dobransky T, Ribeiro FM. Synaptic elimination in neurological disorders. *Curr Neuropharmacol*. 2019;17:1071-1095.
138. Schafer DP, Lehrman EK, Kautzman AG, et al. Microglia sculpt postnatal neural circuits in an activity and complement-dependent manner. *Neuron*. 2012;74:691-705.
139. Daborg J, Andreasson U, Pekna M, et al. Cerebrospinal fluid levels of complement proteins C3, C4 and CR1 in Alzheimer's disease. *J Neural Transm*. 2012;119:789-797.
140. Lian H, Litvinchuk A, Chiang ACA, Aithmitti N, Jankowsky JL, Zheng H. Astrocyte-microglia cross talk through complement activation modulates amyloid pathology in mouse models of Alzheimer's disease. *J Neurosci*. 2016;36:577-589.
141. Czirr E, Castello NA, Mosher KI, et al. Microglial complement receptor 3 regulates brain Aβ levels through secreted proteolytic activity. *J Exp Med*. 2017;214:1081-1092.
142. Wyss-Coray T, Mucke L. Inflammation in neurodegenerative disease—a double-edged sword. *Neuron*. 2002;35:419-432.
143. Wyss-Coray T, Yan F, Lin AH-T, et al. Prominent neurodegeneration and increased plaque formation in complement-inhibited Alzheimer's mice. *Proc Natl Acad Sci*. 2002;99:10837-10842.

SUPPORTING INFORMATION

Additional supporting information can be found online in the Supporting Information section at the end of this article.

How to cite this article: Latif-Hernandez A, Yang T, Butler RR, et al. A TrkB and TrkC partial agonist restores deficits in synaptic function and promotes activity-dependent synaptic and microglial transcriptomic changes in a late-stage Alzheimer's mouse model. *Alzheimer's Dement*. 2024;20:4434–4460. https://doi.org/10.1002/alz.13857